

Laser-driven plasma sources of intense, ultrafast, and coherent radiation

Cite as: Phys. Plasmas **28**, 013105 (2021); doi: [10.1063/5.0031459](https://doi.org/10.1063/5.0031459)

Submitted: 1 October 2020 · Accepted: 8 December 2020 ·

Published Online: 11 January 2021



View Online



Export Citation



CrossMark

Matthew R. Edwards,^{1,2,a),b)}  Nathaniel J. Fisch,^{3,4}  and Julia M. Mikhailova¹

AFFILIATIONS

¹Department of Mechanical and Aerospace Engineering, Princeton University, Princeton, New Jersey 08544, USA

²Lawrence Livermore National Laboratory, Livermore, California 94550, USA

³Department of Astrophysical Sciences, Princeton University, Princeton, New Jersey 08544, USA

⁴Princeton Plasma Physics Laboratory, Princeton, New Jersey 08543, USA

Note: This paper is part of the Special Collection: Papers from the 61st Annual Meeting of the APS Division of Plasma Physics.

Note: Paper NI31, Bull. Am. Phys. Soc. **64** (2019).

^{a)}Invited speaker.

^{b)}Author to whom correspondence should be addressed: edwards78@llnl.gov

ABSTRACT

High-power lasers can deliver extreme light intensities, but avoiding damage in optical components requires large beam sizes, hindering further advances. The use of plasma as a medium for generating and manipulating light avoids the damage thresholds of solid materials and can support extraordinarily bright radiation. We discuss here how parametric plasma amplification and relativistic high-order harmonic generation offer paths to the development of light sources with peak powers beyond the capabilities of solid-state optics.

Published under license by AIP Publishing. <https://doi.org/10.1063/5.0031459>

I. INTRODUCTION

The most powerful lasers operating today can accelerate electrons to GeV energies,^{1–5} generate bright sub-femtosecond x-ray pulses,^{6,7} and reproduce astrophysics at the laboratory scale,^{8,9} yet they are limited to peak powers of 1–10 PW by the material constraints of their component optics. Lasers that can fully explore the ultra-relativistic regime, readily probe non-linear quantum-electrodynamics effects, and take full advantage of new accelerator technology lie beyond the reach of solid-state chirped-pulse-amplification.¹⁰ Substantial further increases in laser peak power will require entirely new approaches.

For sub-picosecond lasers, peak power is limited by the unfocused intensity on post-compression optics—typically on the order of 10^{12} W/cm²—and the expense of large-diameter optical-quality surfaces. The minimum focal spot size is diffraction-limited to the scale of a wavelength, and high-quality wavelength-scale spots can already be achieved for high-power systems. Higher intensities, therefore, require higher peak powers. For example, directly reaching the Schwinger limit (10^{29} W/cm²) in a 1 μ m-diameter spot requires a zettawatt laser (10^{21} W). Using chirped pulse amplification, a zettawatt beam would require gratings and mirrors more than 300 m in diameter. Even an exawatt beam, at 10 m across, is currently unfeasible.

Intensities above 10^{13} W/cm² ionize most materials, so methods to manipulate high-power small-diameter beams will likely require ionized media, i.e., plasma, rather than advances in materials or coatings. Damage thresholds in plasma, which we will use here to mean where performance starts to degrade for increasing intensity, are generally set by the onset of non-linearities. Relativistic effects, for example, limit the intensity that can theoretically be achieved in a plasma amplifier for 1 μ m light to around 10^{18} W/cm²,¹¹ six orders-of-magnitude higher than the solid-state threshold. The orders-of-magnitude difference between the solid-state damage threshold and the intensity-tolerance of plasma offers an opportunity to build more compact and higher-power lasers.

Plasma has several advantages as a photonic medium. (1) Since peak power is limited by plasma non-linearities rather than optical damage, plasmas tolerate high intensities; a plasma optic will have a high damage threshold. (2) Light interacts directly with free electrons, allowing ultrafast response times and readily supporting femtosecond and sub-femtosecond pulses. (3) The free electrons in a classical plasma have continuum energy levels, so plasma optics support broad bandwidths and are in general less sensitive to the laser wavelength than atomic systems. (4) Higher-order non-linearities—accessible without optics damage—allow frequency conversion and other beam

manipulation at high energy flux and peak power. Plasma optics are still an active area of research, rather than a dominant technology, due to the difficulties associated with actual implementation; stability and control can be particular problems, and in many cases, the underlying physics and plasma dynamics are incompletely understood. The step between proof-of-principle experiments and deployable devices requires closing the gap between theory and experiments, as well as increasing demonstrated efficiencies.

The potential advantages of plasmas have led to a range of proposed and implemented plasma optics. Plasma mirrors—which take advantage of the reflectivity of overdense plasma—are used to improve temporal and spatial contrast on high-power beamlines,^{12–15} and generate high-intensity high-order harmonics.^{6,16–24} Plasma amplifiers transfer energy from a high-energy pump to a shorter-duration high-power seed beam, allowing parametric amplification at high intensity and offering a replacement for compression gratings and large crystal amplifiers.^{25–28} High beam energies can also be achieved by combining multiple beams into one using ion-acoustic waves to mediate the interaction.²⁹ Waveplates and polarizers suitable for high-flux operation have also been proposed and demonstrated in plasma.^{30–33} Plasma-based sources of high-frequency light include frequency upconversion from flying mirrors³⁴ and photon acceleration^{35–39} and betatron and Compton x-rays from wakefield accelerated electrons.^{40,41}

Figure 1 shows approximately where these types of radiation sources fall on a plot of wavelength against achievable peak power. High-peak-power lasers are most readily available for near-infrared and visible wavelengths. At shorter wavelengths, alternative sources include high-order harmonic generation (HHG) (gas or plasma based), x-ray lasers based on exciting ions in a plasma, x-ray free electron lasers, and betatron radiation. Demonstrated plasma amplifiers are at the near-infrared wavelengths of the pumps used, although, in principle, the mechanism will work across a wide range of frequencies.

In this paper, we discuss how two particular mechanisms—parametric plasma amplification and relativistic high-order harmonic generation—can advance the development of extremely bright light sources. For parametric plasma amplification, we cover how a simple three-wave picture of plasma amplification extends to encompass a wide range of conditions, including short wavelengths, incoherence, and magnetization. For high-order harmonic generation, we explore how the efficiency depends on the underlying mechanism and how that efficiency can be improved by varying the interaction parameters.

II. RELATIVISTIC HIGH-ORDER HARMONIC GENERATION

The relativistic generation of high-order harmonics from solid-density plasma surfaces is a promising mechanism for producing high-power pulses at wavelengths from the ultraviolet (UV) through soft x-rays, a spectral range that is difficult to reach directly with laser gain media. The creation of attosecond pulses requires broadband light with wavelengths in the UV or shorter. Although there are multiple nonlinearities that can be used to create high-order harmonics—in atomic gases,^{42–47} low-density plasmas,⁴⁸ and solid crystals^{49–51}—the relativistic mechanism of HHG from solid-density plasma surfaces^{6,7,16–19,22–24,52–57} supports the highest driving fluxes and attosecond pulse intensities.

Relativistic HHG (RHHG) requires high intensity light (normalized field $a_0 > 1$, where $a_0 = eE/m_e\omega_L c = 0.84I^{1/2}\lambda$ for intensity I in

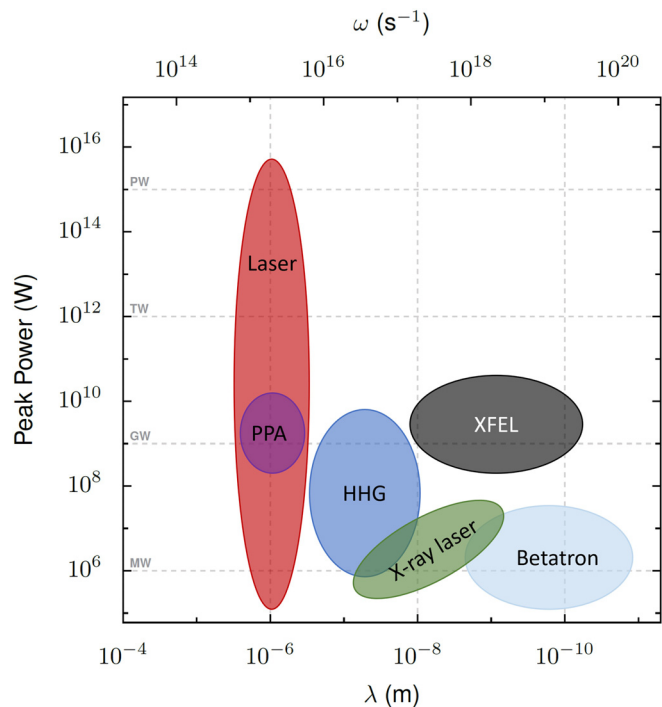


FIG. 1. Approximate ranges of peak powers and wavelengths currently achieved by high-power light sources based on solid-state laser architectures [Ti:sapphire, Nd:glass, and optical parametric chirped pulse amplification (OPCPA)], x-ray free electron lasers, betatron emission from laser-accelerated electrons, x-ray lasers based on excited ions, high-order harmonic generation (HHG), and parametric plasma amplification.

10^{18} W/cm² and wavelength λ in μm , where E is the electric field, ω_L is the laser frequency, c is the speed of light, and e and m_e are the charge and mass of an electron) focused on a solid density surface. The geometry for the experimental study is shown in Fig. 2(a): a high-power short-pulse laser is tightly focused onto a surface, producing harmonics in the direction of specular reflection. The process relies on the highly nonlinear motion of electrons driven by the strong laser and plasma fields; an example trajectory is shown in Fig. 2(b).

There are several models for RHHG, including the relativistic oscillating mirror (ROM),^{16,58} which treats the plasma as a nonlinearly moving reflector, the relativistic electron spring (RES),^{59–61} and coherent synchrotron emission (CSE).^{22,62–65} The ROM model predicts that the relative power in each generated harmonic will scale with the harmonic frequency ω as $\omega^{-8/3}$. CSE, associated with a higher intensity regime, predicts scaling as $\omega^{-4/3}$ —an exponent borne out by particle-in-cell (PIC) simulations—and is the model we explore in depth below for the implications it has on how to maximize the efficiency of the harmonic generation process.

A. Coherent synchrotron emission

In the coherent synchrotron emission (CSE) model of relativistic HHG, high frequency light is emitted by dense bunches of relativistic electrons driven in instantaneously synchrotron-like trajectories

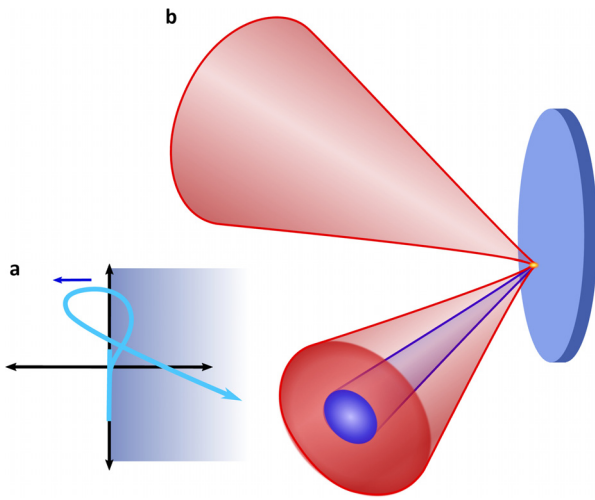


FIG. 2. (a) Schematic of relativistic high-order harmonic generation, including the incident laser, target, and reflected harmonics. (b) Example trajectory followed by electrons in the CSE regime.

[Fig. 2(b)] such that the position of the bunch relative to the target normal (x) is

$$x(t) = \beta_x t \omega_L + \frac{\alpha + 1}{3} (t \omega_L)^3, \quad (1)$$

and the transverse current is linear,

$$j_y(t) = \alpha_0 t \omega_L, \quad (2)$$

where $\beta_x = v_x/c$ is the normalized velocity component, $t=0$ is the time when the peak of the attosecond pulse is emitted, and $\alpha_{0,1}$ are constants. The emission spectrum may, then, be written as^{62,64}

$$I(\omega) \propto |\tilde{f}(\omega)|^2 \omega^{-4/3} \left\{ \text{Ai}' \left[\left(\frac{\omega}{\omega_\gamma} \right)^{2/3} \right] \right\}^2, \quad (3)$$

where $\omega_\gamma = \sqrt{8\alpha_1\gamma^3}$, $\gamma = 1/\sqrt{1-v^2/c^2}$ is the Lorentz factor at the emission time, Ai' is the derivative of the Airy function of the first kind, and $\tilde{f}(\omega)$ is the Fourier transform of the shape function f , which describes the spatial distribution of the electron bunch. The salient feature of the CSE model is that for harmonic wavelengths longer than the bunch thickness ($\tilde{f} = 1$) and frequencies lower than the cutoff frequency ($\omega < \omega_\gamma$), the spectral power scales as $\omega^{-4/3}$, much shallower than the $\omega^{-8/3}$ scaling of ROM. This power-law exponent sets the maximum efficiency of the CSE model, although observed HHG spectral scaling is often much lower. This can occur because the total spectrum is emitted by a large number of electrons, and at lower efficiencies, only a small fraction of them may reach the maximum observed velocity. Slower electrons will have cutoffs at lower frequencies and only contribute to lower-order harmonics, leading to a steeper decay in the total spectrum.

The coherent synchrotron electron trajectories are created by the combination of the laser electric and magnetic fields and the plasma electric charge separation field. The laser electric field accelerates electrons to relativistic velocities, the plasma electric field prevents the

electrons from being carried along with the laser and produces a longitudinal force, and the laser magnetic field turns the electrons, coupling the electric fields together. This balance of forces produces trajectories like those in Fig. 2(a), with a characteristic shape that can be found across a wide range of laser and plasma conditions.⁶⁴

Figure 3 shows the Lorentz factor of selected electrons in an emitting bunch as a function of their advanced time—the time when radiation associated with that trajectory will arrive at a far boundary. These trajectories have been found using one-dimensional particle-in-cell (PIC) simulations. The profile is not symmetric; the left side, corresponding to the leading edge of arriving radiation, is much sharper than the right. For reasonably high frequencies, we can treat the left edge as infinitely sharp and the right side as decaying infinitely slowly, i.e., a Heaviside step function. Although the right side does not stay constant, the change is sufficiently slow that the high-frequency components of the emitted radiation do not add constructively: only the leading edge provides a contribution. This approximation for the shape function, when Fourier transformed, adds a factor ω^{-2} to the spectrum so that for frequencies satisfying $\omega < \omega_\gamma$ but with wavelengths longer than the bunch width ($\omega > \omega_b$), the spectrum scales as $\omega^{-10/3}$. For $\omega > \omega_\gamma$, the spectrum falls off exponentially. In Fig. 3(b), all three of these scaling regimes can be observed, but in general, they do not have to be well separated. If $\omega_B \geq \omega_\gamma$, the effect of the finite

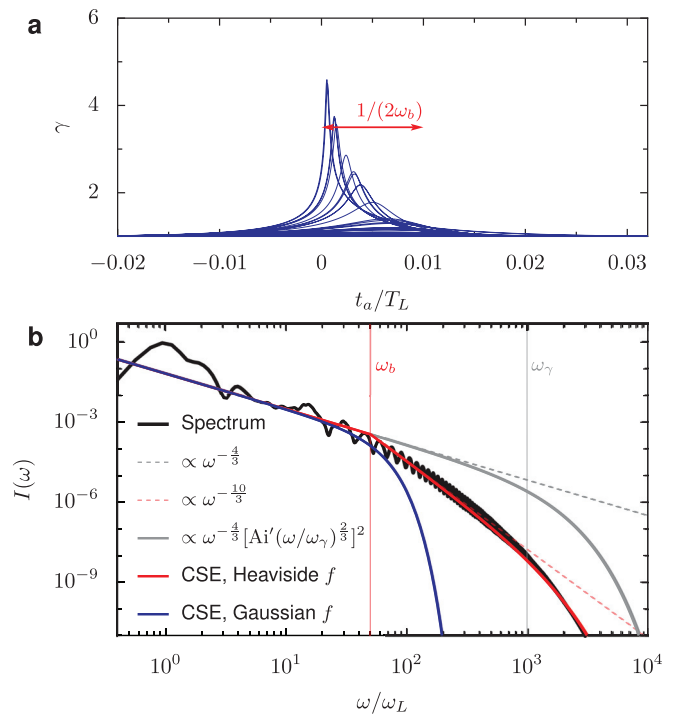


FIG. 3. Electron trajectories and resulting HHG spectrum, as calculated with one-dimensional PIC simulations (EPOCH). (a) The Lorentz factor of electrons, which emit radiation plotted against the arrival time of that radiation at a distant observer. (b) The spectrum as a function of frequency normalized by laser frequency (ω_L) of the associated radiation compared to variants of the CSE model and power-law fits, showing the three distinct regions of spectral behavior. The frequencies ω_b and ω_γ are marked. For both (a) and (b), the laser angle of incidence (θ_L) is 30° , the laser is single cycle ($\tau = 3$ fs and $\lambda = 800$ nm), $a_0 = 40$, and $N = 200$.

bunch width will be hidden by the much stronger effect of the γ -dependent cutoff.

The Lorentz factor cutoff (ω_γ) depends on the maximum Lorentz factor reached by an electron in the bunch and directly results from the limit on radiation frequencies produced by an accelerating electron of a particular momentum. Unlike the trajectories themselves, which depend on a_0/N , the Lorentz factor has an additional proportionality to a_0 , so increasing ω_γ requires higher intensity.

B. Efficiency

Under ideal conditions, the CSE mechanism should be able to convert near-infrared light to a continuum of high frequencies up to multi-keV x-rays with an efficiency $\eta_\omega = C\omega^{-4/3}$, where the conservation of energy gives a maximum coefficient⁶⁶ $C = 1/3$. However, efficiencies observed in simulations and experiments are lower than this limiting case. We will focus here on how choice of parameters influences efficiency rather than on how experimental deviations from targeted conditions result in lower than expected yields.

The dominant parameters that determine the regime of HHG are the laser intensity (represented by a_0) and the plasma density (here normalized by the critical density: $N = n_e/n_c$, where $n_c = m_e\omega_L^2/4\pi e^2$). For RHHG, we must at least satisfy $a_0 > 1$ (relativistic) and $N > 1$ (overdense, reflective plasma). In the relativistic limit ($a_0 \gg 1$), electron dynamics are determined by the similarity parameter S ($a_0/N = 1/S$), which can be derived from the Vlasov–Maxwell equations.^{67–69} As shown in Fig. 4, the efficiency of the process for many values of a_0 and N can be determined relatively accurately by considering only a_0/N . This leaves us with two limits: for $a_0/N \ll 1$, the laser is too weak relative to the plasma field strength to drive a strong plasma response. For $a_0/N \gg 1$, the plasma is relativistically transparent, and the laser will bore a hole through the plasma rather than reflecting from the surface. Efficient RHHG requires that the laser and plasma field strengths are comparable so that the forces balance

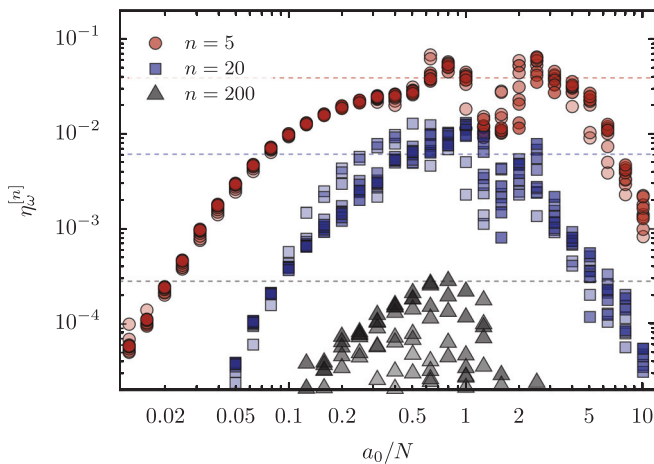


FIG. 4. Simulations of the efficiency ($\eta_\omega^{[n]}$ is the reflected energy in harmonic n divided by total incident energy) of RHHG. Points indicate the fraction of light converted to the n th harmonic for $n = 5, 20$, and 200 at $\theta_L = 45^\circ$. a_0 and N are varied ($1 < a_0 < 100$), ($N > 1$), and the efficiency $\eta_\omega^{[n]}$ is plotted against a_0/N . The results are based on one-dimensional PIC simulations (EPOCH). Driving pulses are single cycle, and there is no gradient on the target surface.

each other throughout the generation process; efficiency rapidly drops for both $a_0/N \gg 1$ and $a_0/N \ll 1$.

For 800-nm light, most fully ionized solids have values of N between 200 and 500 (e.g., fused silica). Available laser systems usually provide $a_0 < 30$, so HHG experiments are conducted in the regime $a_0/N < 1$. To increase the value of a_0/N , we can increase laser intensity and decrease density, or, noting that $a_0 = eE/m_e\omega c$ and $N = 4\pi e^2 n_e/m_e\omega^2$ so that $a_0/N \propto \omega$, we can increase the laser frequency at fixed intensity. Although higher-power lasers are under construction, reaching higher intensities is difficult and expensive, so methods for adjusting S by changing either density or frequency are important.

1. Density

A reduction in density to increase a_0/N can be achieved by directly using a lower-density solid, replacing semi-infinite thick targets with thin foils, or producing a finite plasma density gradient on the interaction surface. Each of these approaches reduces the plasma restoring force, enabling the laser field more effectively manipulate surface electrons.

Most RHHG experiments are conducted with near-infrared light, either 800 nm or near $1 \mu\text{m}$, where standard solid-density materials have values of N of order 10^2 when fully ionized and gases have $N < 1$. RHHG requires an optical quality front surface, so gas targets are less suitable. Certain materials offer lower values of N than fused silica, including polystyrene,⁷⁰ lithium ($N = 75$), and frozen hydrogen. Although lithium and cryogenic targets are substantially more difficult to work with than glass, they offer substantial gains in efficiency, as shown in Fig. 5. In Fig. 5(a), reflected HHG spectra are shown for two different densities; $N = 75$ leads to high-order harmonics one to two orders of magnitude more powerful than a target with $N = 500$. Figure 5(b) shows how this difference in efficiency changes with laser intensity and that under these conditions and all reasonable laser field strengths, the lower density target leads to more efficient harmonic generation.

Foams are an alternative to low density solids, providing controllable low average densities. Although foams have been used in nanosecond laser experiments⁷¹ and are viable for longer pulses, RHHG imposes more stringent requirements on foam properties, especially homogeneity. The surface must be optically smooth on a scale comparable to the harmonics of interest, and together with micrometer-scale focal spots, this means that we need the scale length of the foam voids w to be much smaller than the laser wavelength: $w \ll \lambda$. The femtosecond driving pulse duration means that the foam density will not evolve substantially during the interaction, so the gradual smoothing out of density that can happen on nanosecond timescales must be separately induced if required.

A lower effective density can also be created using thin foils (thickness $d \ll \lambda$) rather than a thick ($d > \lambda$) target. Although the target density is still high, the thinness limits the total charge, and the relevant nondimensional parameter becomes^{72–74}

$$\eta = f\left(\frac{ND}{a_0}\right), \quad (4)$$

where $D = d/\lambda$ is the normalized target thickness and η is the efficiency. As shown in Fig. 6, the efficiency of harmonic conversion can

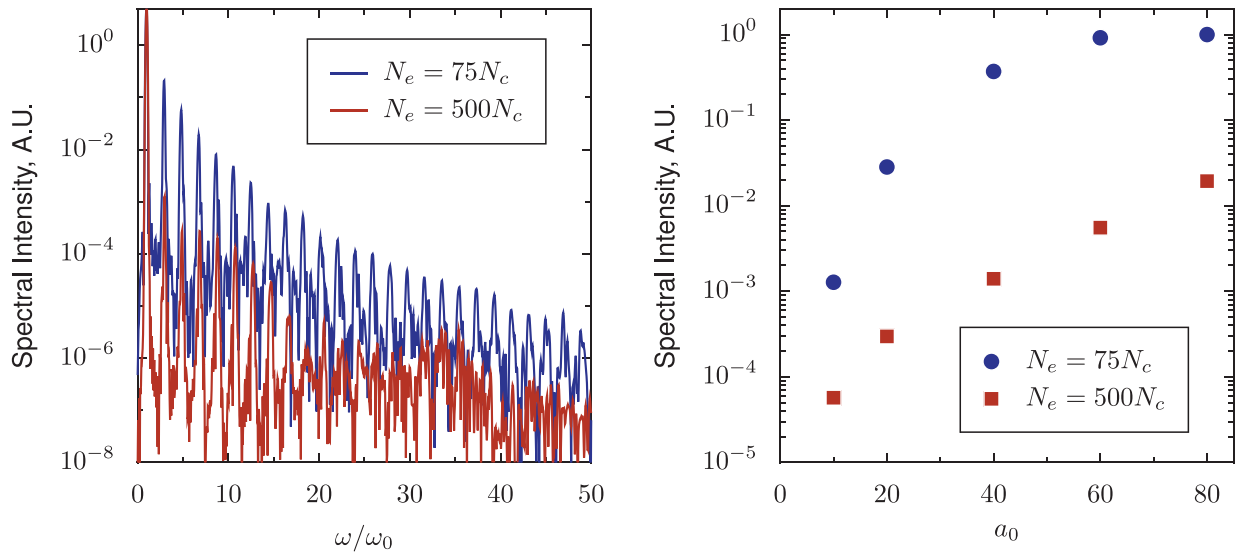


FIG. 5. Effect of plasma density on HHG efficiency. (a) A lower density target ($N = 75$) produces harmonics more efficiently than one with higher density $N = 500$ at $a_0 = 20$ and $\theta_L = 0^\circ$. The results are from 1D PIC simulations (EPOCH). (b) Efficiency of conversion to the spectral range $5 < \omega < 60$ for varied a_0 and both $N = 75$ and $N = 500$. Note that both plots are in normalized (arbitrary) units.

be substantially increased for thin targets, and interactions at the same value of ND/a_0 and other fixed parameters will tend to have the same efficiency. Ultrathin targets also lead to higher Lorentz factors at the same driving a_0 since the incident and reflected electric fields do not cancel completely at the surface,⁷⁴ leading to a larger value of the ω_γ cutoff. This advantage is offset by the increased width of the driven electron bunches for ultrathin targets, which can approach a significant fraction of the laser driving frequency. This increased width means that the shape factor plays a role in the spectral shape at lower

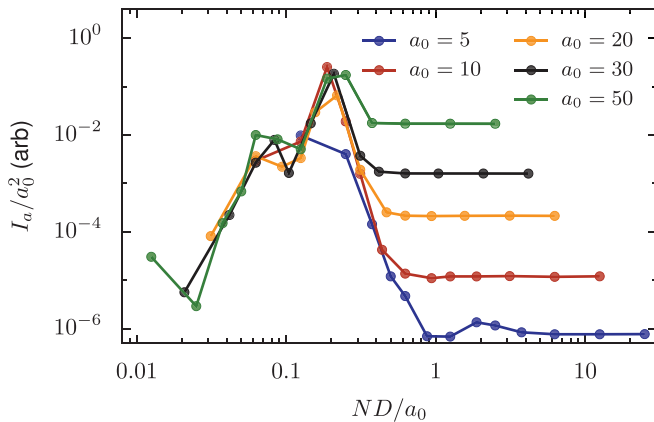


FIG. 6. The efficiency of RHHG, measured here as the normalized ratio of attosecond pulse intensity to incident laser intensity as a function of plasma density N , laser field strength a_0 , and target thickness D , showing that for thin targets ($D \ll 1$), the efficiency of the process varies only with the ratio ND/a_0 , and that for $ND/a_0 \approx 0.2$, the efficiency reaches a maximum. The results are from 1D PIC calculations (EPOCH). N is fixed at 500, and a_0 and D are varied. The driving pulse is single-cycle, the angle of incidence is 30° , and the attosecond pulse intensity is found by considering harmonics between $3 < \omega/\omega_L < 30$.

maximum frequencies, leading to an earlier transition to $\omega^{-10/3}$ scaling and lower efficiencies for thin foils compared to maximum that can be achieved for thicker targets.

A finite plasma density gradient is one further way to manipulate the effective density of the interaction. A sharp plasma surface heated by a laser pulse will self-similarly expand into free space, producing a density gradient that can be approximated as exponential: $N(x) \propto e^{x/L}$. The effect of a finite gradient has been explored both computationally and experimentally,^{54,55} with ideal gradient scale lengths found in the range $L/\lambda = 0.1 - 0.2$. The key advantage of a gradient is that the laser will reflect near the relativistically reduced critical density, rather than at the peak plasma density, so that near the interaction point, $a_0/N \approx 1$, even for very dense solids. Although the shape of the gradient also affects the details of the interaction, the dominant contribution to increased efficiency is the decreased density.

2. Coherent control: Frequency

An alternative method for controlling efficiency—hinted at by the relationship $a_0/N \propto \omega$ —is to manipulate the frequency composition of the driving laser pulse. Doubling the laser frequency ($\omega \rightarrow 2\omega$) at fixed laser intensity will double a_0/N , leading to higher efficiency, a result that follows from the approximate empirical relationship between intensity and a_0/N for $a_0/N < 1$,

$$\frac{I_{\text{atto}}}{I_L} \propto \left(\frac{a_0}{N}\right)^q = \left(\frac{eE}{m\omega_L c} \cdot \frac{m\omega_L^2}{4\pi n_e e^2}\right)^q \propto \omega_L^q. \tag{5}$$

However, for beams containing two distinct colors, increases in efficiency can be much larger than those achieved with either ω or 2ω light separately, with the relative phase between the two colors playing a dominant role in the new efficiency.^{57,75} This is an indication of the importance of the driving waveform as something that can be used

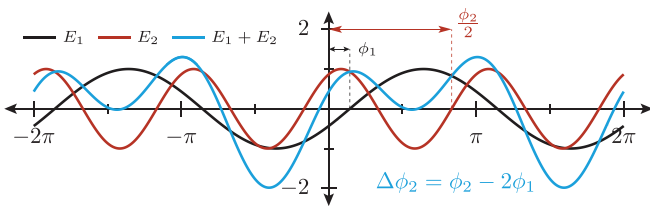


FIG. 7. Schematic of fields in a two-color beam. The definitions of each phase (ϕ_1 , ϕ_2) and relative phase ($\Delta\phi_2$) for a two-color beam, where the second field (E_2) has twice the frequency of the fundamental (E_1), are given. The non-sinusoidal shape of $E_1 + E_2$ is important for the relativistic dynamics of HHG.

both to increase efficiency and improve our understanding of the underlying mechanism. Figure 7 shows how the electric fields of the two colors add together to form a complex nonsinusoidal waveform.

In a two-color beam, we can control the energy fraction in each color and the relative phase ($\Delta\phi$) between them.⁷⁶ Figure 8 illustrates the substantial change in harmonic generation efficiency, which can

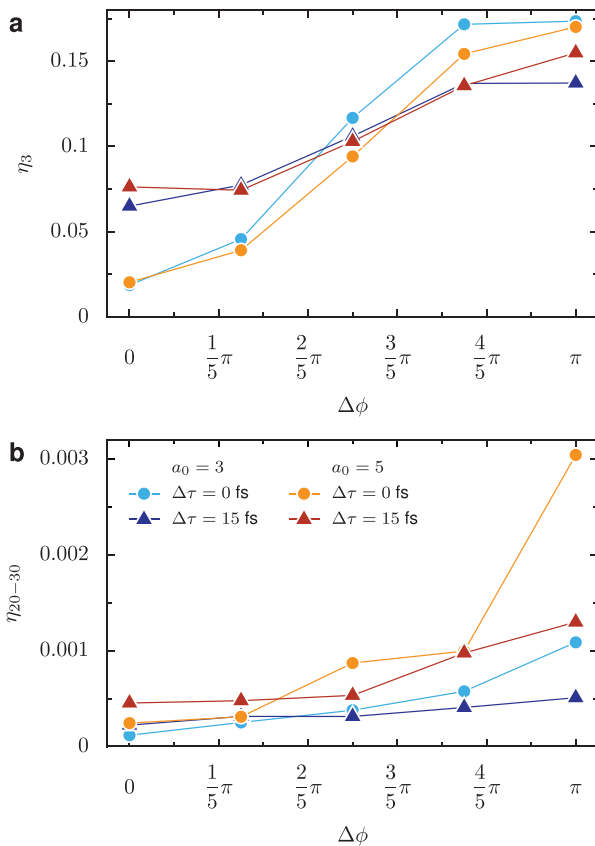


FIG. 8. Effect of the relative phase ($\Delta\phi$) between two color components on high-order harmonic generation for experimentally reachable conditions, including the effect of a relative group delay between the fundamental and second harmonic ($\Delta\tau$). (a) Absolute energy conversion efficiency to the third harmonic. (b) Fraction of energy converted to frequency interval from $\omega/\omega_L = 20$ to $\omega/\omega_L = 30$. These simulations were conducted with $\theta_L = 45^\circ$, $N = 350$, $a_0 = 3, 5$, $\tau_{FWHM} = 25$ fs, the plasma density gradient scale length $L/\lambda = 0.05$, the ratio of ion to electron masses $m_i/m_e = 3672$, and the fraction of light in the second harmonic $W_2/W = 0.1$.

result when the relative phase between component frequencies in a two-color beam is changed. Even for relatively low intensities ($a_0 = 3$), a small fraction (10%) of conversion to second harmonic can measurably affect both low-order (third harmonic) and relativistic ($\omega > 20\omega_L$) harmonic generation. As should be expected, this effect decreases if the envelopes of the fundamental and second harmonic are not perfectly matched; mismatch in group delay between the colors decreases the strength of the effect, as shown by the difference between $\Delta\tau = 0$ and $\Delta\tau = 15$ fs in Fig. 8.

We can use multi-color beams (n colors, with $n > 2$) to understand the mechanism of efficiency enhancement via subcycle waveform modification since arbitrary waveforms can be constructed by the superposition of harmonics. To address the high-dimensional parameter space for beams defined by n phases and $n - 1$ energy fractions, previous work⁷⁷ used a genetic algorithm to find the highest-efficiency driving waveforms, arriving at shapes like that shown in Fig. 9. In this waveform, the field transition from its maximum negative to maximum positive value occurs over a time period comparable to the relativistic plasma period, corresponding to a matching of the laser and plasma forces. The enhancement seen for two-color beams occurs because when appropriately phased, a two-color beam will be closer to this driving waveform than a beam of either color individually. It is also why there is less room for improvement via waveform manipulation when the laser intensity and plasma density are already well-matched.

Although producing a multicolor beam with a controllable phase is not generally possible at relativistic intensities, such a beam could, in principle, be generated by and used in a multipass configuration of high-order-harmonic mirrors,^{78–83} where the harmonics reflected from an initial relativistic plasma mirror subsequent interactions. As illustrated in Fig. 10(a), a multipass configuration could be built by refocusing a harmonic beam onto a second target. Alternatively, the beam may be focused onto two close, sequential surfaces, although the evolution of the Guoy phase places a restriction on the spacing between the interactions.⁸² In both configurations, multipass

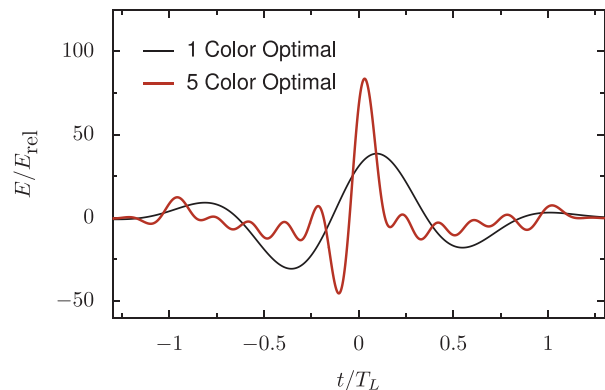


FIG. 9. The waveform associated with the highest harmonic generation efficiency constructed from the first five harmonics of the fundamental driving pulse (red), compared to a single frequency pulse (black). The optimal pulse shape was found from a genetic algorithm optimization of harmonic generation efficiency found in 1D PIC simulations. The key feature of the optimized pulse shape is the transition from the negative to positive electric field near $t = 0$, which has an effective frequency that matches the relativistic plasma frequency.

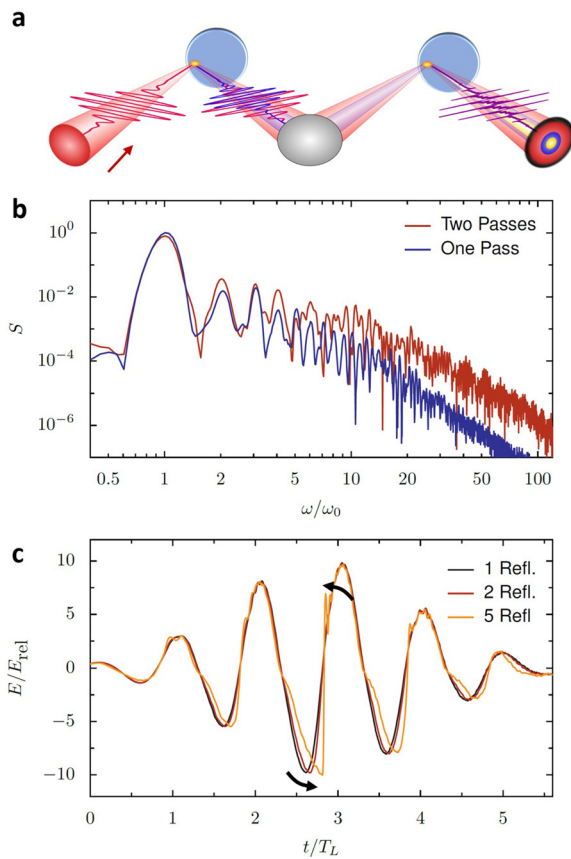


FIG. 10. (a) Schematic of a multi-pass HHG interaction. (b) The reflected spectrum of light after one and two passes at $\theta_L = 15^\circ$, $a_0 = 30$, $N = 200$, and $\tau = 5$ fs calculated with one dimensional PIC simulations (BOPS). The laser has an 800-nm fundamental wavelength. (c) The reflected electric field of a short pulse laser after 1, 2, and 5 passes, showing the reshaping of the field around the transitions in field direction. E_{rel} is the field corresponding to $a_0 = 1$ for the fundamental frequency.

enhancement [Fig. 10(b)] relies on the closeness of the reflected harmonic relative phases to those required for efficiently driving HHG. Figure 10(c) shows how the electric field of the reflected beam steepens with each subsequent pass; as the local frequency during this transition approaches the relativistic plasma frequency, the efficiency of the interaction increases. Fundamentally, the reflected pulses are phased correctly because the interaction produces attosecond pulses, where the high frequency components of the reflected light add coherently.

There are restrictions on multipass configurations that follow from the phase requirements for driving HHG. For example, for finite angles of incidence, subsequent mirrors must continue to reflect the pulses in the same direction, rather than alternate between mirror directions; in an alternating configuration, the field components associated with even harmonics will have the opposite sign (180° out of phase) as that required for efficient generation, leading to suppression. Furthermore, losses with each interaction mean that although in a perfectly reflecting system a large number of passes can produce very high efficiencies,⁷⁹ the practical number of interactions, which will continue to produce enhancement, is limited. In an experimental

demonstration of a two-color beam from a plasma mirror, around 40% of the incident energy was not reflected in either color.⁸³ Whether the efficiency gains due to the improved waveform makeup for the reduced intensity depends on the specific parameters of the interaction under consideration; in regions where enhancement is large, even substantial drops in driving energy are offset by the improved field shape. In Fig. 8, a two-color beam at $a_0 = 5$ with poorly phased colors ($\Delta\phi = 0$) is less efficient at driving both the third and higher-order harmonics than a beam at $a_0 = 3$ (64% less energy) with an ideal relative phase ($\Delta\phi = \pi$) and produces less absolute energy in the harmonics despite the higher driving energy.

Taken together, the advantage of waveform manipulation strategies is that they allow available laser intensities and target densities to be moved into a more efficient regime and concentrate more on the laser field energy into those times of the waveform, which primarily contribute to driving emitting electrons. As a result, a multicolor beam can almost reach the highest efficiencies theoretically possible for relativistic high-order harmonic generation.

III. PLASMA AMPLIFIERS

An ideal plasma amplifier would replace both the compression grating and the final stage amplifier of a solid-state system, producing femtosecond (Raman) or picosecond (Brillouin) compressed pulses at unfocused intensities above 10^{17} W/cm² for $\lambda = 1 \mu\text{m}$. The basic mechanism (Fig. 11) relies on coupling between three waves: a plasma wave and the electromagnetic waves of a pump laser and a seed laser. This coupling transfers energy from the long-duration high-energy pump laser to the short-duration high-power seed, provided that the pump and seed satisfy wavevector matching conditions ($\omega_{\text{pump}} = \omega_{\text{seed}} + \omega_{\text{plasma}}$, $\mathbf{k}_{\text{pump}} = \mathbf{k}_{\text{seed}} + \mathbf{k}_{\text{plasma}}$).

Theory, numerical models, and large-scale simulations have predicted that reaching close-to-relativistic seed intensities inside plasma amplifiers is possible, with the amplified seed peak powers often exceeding the corresponding pump power by several orders of magnitude and energy transfer efficiencies of 90% or higher. However, experimental performance (Fig. 12) tends to be lower, with demonstrated seed peak powers at most an order of magnitude higher than the pump. Apart from a groundbreaking recent study showing 20% energy-transfer efficiency for a Brillouin amplifier,⁸⁴ the demonstrated efficiency has been lower than a few percent. Although no conclusive reason for the discrepancy between the simulations and experiments has been established, possible explanations include insufficient treatment of kinetic processes in theory and experimental imperfections—like mismatched alignment between the pump and seed—which are not captured in simulations, and the difficulty of establishing a large plasma of sufficient uniformity for the amplification process to be efficient everywhere.

A. Mechanism

The simplest model that reproduces amplification dynamics is based on the Maxwell-fluid equations, where the plasma is treated as an electron fluid and an ion fluid. Although powerful, this approach does not directly include kinetic and non-continuum effects, which are either neglected or modeled with additional terms.

Let \mathbf{A}_1 represent the vector potential of the seed beam and \mathbf{A}_2 the vector potential of a counterpropagating pump. The equation for the seed beam is

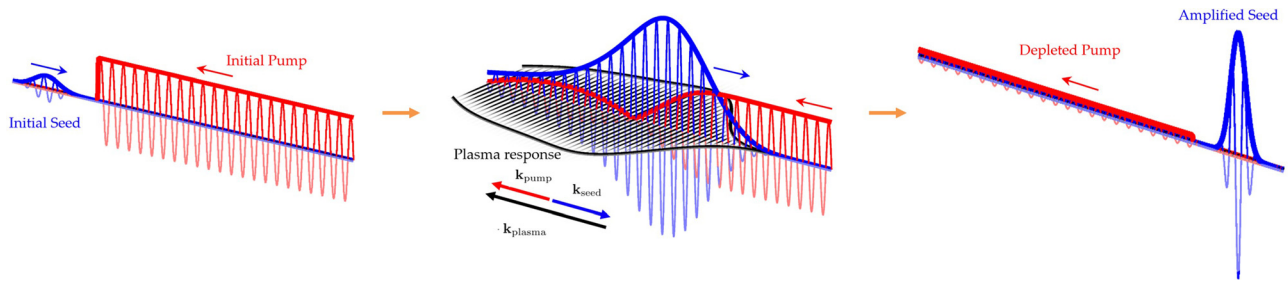


FIG. 11. Schematic of the plasma amplification process. A low energy short seed pulse crosses a longer high energy pump beam in a plasma, creating a plasma wave, where $k_{\text{plasma}} = k_{\text{pump}} - k_{\text{seed}}$. The final amplified seed pulse contains a significant fraction of the pump energy but maintains the short seed envelope.

$$\left[\partial_t^2 - c^2 \partial_x^2 + \omega_{pe}^2 + \nu_1 \partial_t \right] \mathbf{A}_1 = -\omega_{pe}^2 \frac{n_{e,1}}{n_{e,0}} \mathbf{A}_2, \quad (6)$$

where ν_1 represents the damping of the wave, ω_{pe} is the plasma frequency, $n_{e,1}$ is the unperturbed plasma density, and $n_{e,1}$ is the perturbed component. An equivalent equation may be written for the pump as follows:

$$\left[\partial_t^2 - c^2 \partial_x^2 + \omega_{pe}^2 + \nu_2 \partial_t \right] \mathbf{A}_2 = -\omega_{pe}^2 \frac{n_{e,1}}{n_{e,0}} \mathbf{A}_1. \quad (7)$$

Both of these equations depend on how the modulation of the electron density ($n_{e,1}$) responds to the seed and pump fields. Note that we can neglect the direct ion contribution to Eqs. (6) and (7) because the ions are much heavier than the electrons, an assumption that would break

down, for example, in an electron-positron plasma.^{97,98} Depending on the plasma conditions and the wavelength separation, the evolution of the electron number density may be dominated by the Langmuir wave [stimulated Raman scattering (SRS)],^{27,86,88–91,99–109} an ion-acoustic wave [stimulated Brillouin scattering (SBS)] or ion-acoustic quasimode (strongly coupled stimulated Brillouin scattering),^{26,28,84,93–95,97,109–117} a non-collective super-radiant electron response,^{96,118} or, in magnetized plasma, a kinetic Alfvén wave¹¹⁹ or an upper hybrid wave.¹²⁰

The system of equations may be closed by writing an expression for the evolution of the plasma. For stimulated Raman scattering, where the pump and seed are separated by the plasma frequency, this is

$$\left[\partial_t^2 - 3v_e^2 \partial_x^2 + \omega_{pe}^2 + \nu_3^R \partial_t \right] \frac{n_{e,1}}{n_{e,0}} = \frac{e^2}{m_e^2 c^2} \partial_x^2 (\mathbf{A}_1 \cdot \mathbf{A}_2), \quad (8)$$

where ν_3^R represents the damping of the Langmuir wave, which could be Landau damping at low density and high temperature or collisional damping at high density and low temperature.¹¹⁷ For stimulated Brillouin scattering, the full expression may be written as follows:

$$\left[\partial_t^2 - c_s^2 \partial_x^2 + \nu_3^B \partial_t \right] \frac{n_{e,1}}{n_{e,0}} = \frac{Ze^2}{m_e m_i c^2} \partial_x^2 (\mathbf{A}_1 \cdot \mathbf{A}_2), \quad (9)$$

which similarly has a damping term.

With normalized units (time $\tilde{t} = t\omega_2$ and position $\tilde{x} = x\omega_2/c$), the three wave equations for the pump and seed may be written as follows:

$$[\partial_{\tilde{t}} + \tilde{\nu}_1 \partial_{\tilde{x}} + \tilde{\nu}_1] a_1 = -\frac{1}{4} \frac{\omega_2}{\omega_1} N(n_3^* a_2), \quad (10)$$

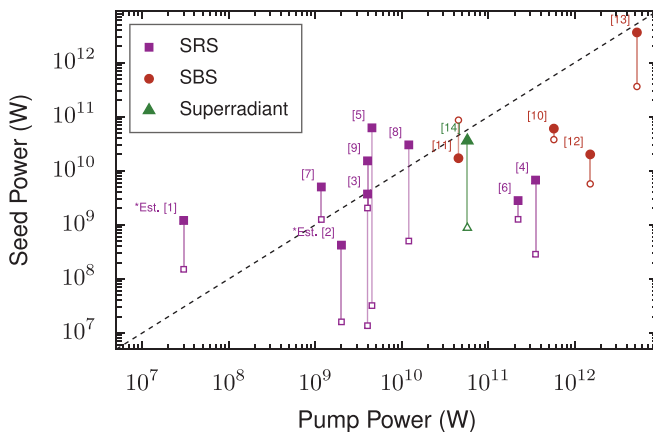
$$[\partial_{\tilde{t}} + \tilde{\nu}_2 \partial_{\tilde{x}} + \tilde{\nu}_2] a_2 = \frac{1}{4} N(n_3 a_1), \quad (11)$$

where $a_{1,2} = eA_{1,2}/m_e c$, the damping rates are normalized as $\tilde{\nu}_{1,2} = \nu_{1,2}/\omega_2$, and the group velocity of light is normalized as $\tilde{v}_{1,2} = k_{1,2}c/\omega_{1,2} = (1 - \omega_{pe}^2/\omega_{1,2}^2)^{1/2}$. The expressions for the plasma response in SRS may be rewritten as follows:

$$[\partial_{\tilde{t}} + v_3 \partial_{\tilde{x}} + \tilde{\nu}_3^R] n_3 = -\frac{1}{4} \frac{1}{\sqrt{N}} \frac{c^2 k_3^2}{\omega_2^2} (a_1^* a_2), \quad (12)$$

and the full expression for SBS is

$$\left[\frac{i}{2} \frac{\omega_2}{\omega_3} \partial_{\tilde{t}}^2 + \partial_{\tilde{t}} + \tilde{\nu}_3^B \right] n_3 = -\frac{1}{4} \frac{Z m_e \omega_2}{m_i \omega_3} \frac{c^2 k_3^2}{\omega_2^2} (a_1^* a_2), \quad (13)$$



- | | |
|----------------------------------------------------------------------|---------------------------------------------------------------------------|
| [1] Y. Ping, et al, <i>Phys. Rev. E</i> 66 046401, 2002. | [8] D. Turnbull, et al, <i>Phys. Plasmas</i> 19 , 073103, 2012. |
| [2] Y. Ping, et al, <i>Phys. Rev. Lett.</i> 92 175007, 2004. | [9] X. Yang, et al, <i>Sci. Rep.</i> 5 , 13333, 2015. |
| [3] W. Cheng, et al, <i>Phys. Rev. Lett.</i> 94 045003, 2005. | [10] L. Lancia, et al, <i>Phys. Rev. Lett.</i> 104 , 025001, 2010. |
| [4] R. Kirkwood, et al, <i>Phys. Plasmas</i> 14 113109, 2007. | [11] E. Guillaume, et al, <i>HPLaser</i> 2 , e33, 2014. |
| [5] J. Ren, et al, <i>Phys. Plasmas</i> 15 , 056702, 2008. | [12] L. Lancia, et al, <i>Phys. Rev. Lett.</i> 116 , 075001, 2016. |
| [6] Y. Ping, et al, <i>Phys. Plasmas</i> 16 , 123113, 2009. | [13] J.-R. Marquès, et al, <i>Phys. Rev. X</i> 9 , 021008, (2019). |
| [7] G. Vieux, et al, <i>New J. Phys.</i> 13 , 063042, 2011. | [14] M. Dreher, et al, <i>Phys. Rev. Lett.</i> 93 , 095001, 2004. |

FIG. 12. Experimental demonstrations of parametric plasma amplification. The initial (open squares) and final (closed squares) seed powers are plotted against the pump powers; for points above the dashed line, the seed peak power exceeds the pump power. Some points (Est) use final peak powers based on estimated, rather than measured, final pulse durations. Values were extracted from Refs. 27 and 84–96.

where the second derivative term on the left hand side may be neglected in the weakly coupled regime and the first derivative term may be neglected in the strongly coupled regime.²⁸ These equations may be evaluated numerically or, in some limits, analytically.

For Raman and Brillouin amplification, the process of amplifying a seed pulse can be divided into two distinct regimes. In the linear regime [Fig. 13(a)], the seed is small compared to the pump, and the pump is not measurably depleted. As a result, the seed grows exponentially, with the pulse lengthening and the peak moving slower than the group velocity of light. In the nonlinear regime [Fig. 13(b)], pump depletion is substantial, so only the leading edge of the seed is amplified. The seed shortens in time, and its peak travels faster than the group velocity as the total energy in the pulse increases at a constant rate. This is also referred to as the π -pulse regime.²⁵

1. Growth rate

The growth rate of the instability is an important measure because it determines how quickly the nonlinear regime will be reached and for how long the desired energy-transfer mechanism will outperform competing instabilities. In general, a higher growth rate is desirable for improved amplifier performance. Using the three wave model, we can derive an effective growth rate in the linear regime for both Raman and Brillouin amplification in the presence of substantial damping.

Extending the quasitransient backward Raman amplification approach to include damping of the seed, we can write an asymptotic (the influence of initial conditions goes to zero as $t \rightarrow \infty$), linear-regime (pump intensity constant) expression for the growth rate of a Raman-amplified seed by finding a solution to the coupled equations,

$$[\partial_t + \tilde{\nu}_1 \partial_x + \tilde{\nu}_1] a_1 = K_1 n_3, \tag{14}$$

$$[\partial_t + \tilde{\nu}_3] n_3 = K_3 a_1, \tag{15}$$

of the form $a_1(z, t) = \alpha(\xi) e^{k\xi t}$, $n_3(z, t) = \eta(\xi) e^{k\xi t}$, where $\xi = \frac{\tilde{x}}{vt}$. This yields the general expression

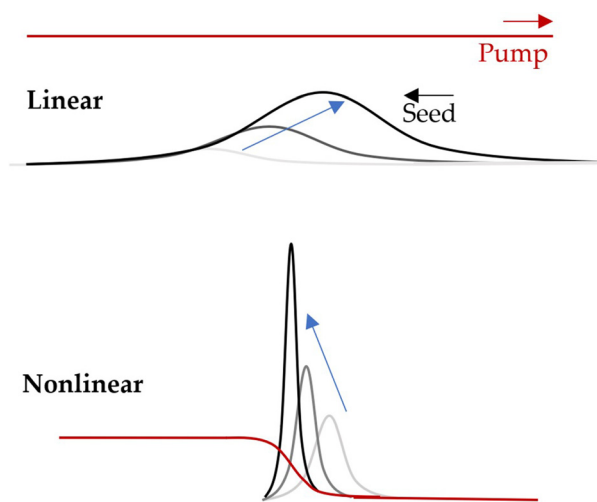


FIG. 13. Illustration of (a) the linear (constant pump) and (b) nonlinear (pump depletion) regimes of plasma amplification.

$$\kappa = \frac{1}{2} \sqrt{4K_1 K_3 + (\tilde{\nu}_3 - \tilde{\nu}_1)^2} - \frac{\tilde{\nu}_3 + \tilde{\nu}_1}{2}. \tag{16}$$

This expression is the same for weakly coupled SBS. The expression for the full form of SBS requires solving a cubic expression for κ .¹¹⁷

B. Extension to new regimes

The theory of parametric plasma amplification has been well explored for near-infrared high-quality pump beams in uniform unmagnetized plasma. Below, we describe how relaxing some of those constraints affects the amplification process and, in particular, how that might affect the prospects for usable plasma amplifiers. Specifically, we discuss the effects of incoherent pump beams, x-ray wavelengths, and strongly magnetized plasmas.

1. Incoherent amplification

A key useful feature of parametric amplification is that it does not require the pump beam to be strictly coherent and uniform, which has previously been shown to be true in non-plasma media.^{121–123} In plasma,¹⁰⁸ the amplification process will tolerate a substantial degree of incoherence in the pump. Although the amplification dynamics are adjusted by pump's finite coherence time, the nonlinear amplification regime, in particular, is not strongly affected by coherent structures.

Figure 14 shows a PIC simulation of a seed pulse being amplified by a pump, which is only coherent on a timescale comparable to the envelope of the seed itself, as indicated by the pump envelope modulations. Despite this high degree of incoherence, the seed rapidly amplifies, and the final intensity is comparable to that found for a fully coherent pump at the same average power. The leading edge of the seed—within a pump coherence time of the front edge—does not experience the incoherence of the pump, as the plasma wave locally forms with the correct phase to match the seed and pump. By the trailing edge of the seed, the pump and plasma wave, which travel at

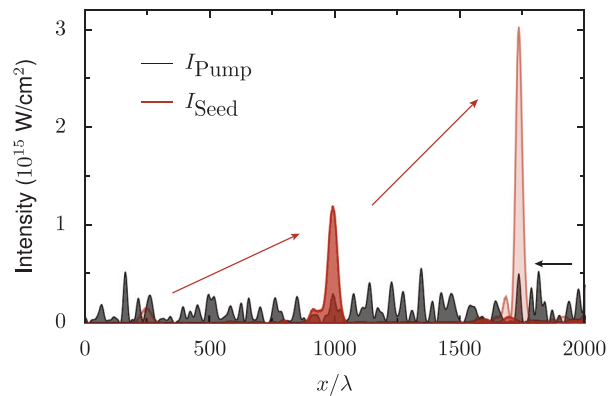


FIG. 14. One dimensional PIC simulation (EPOCH) of the growth of a seed pulse (red) in an incoherent pump beam (black) via Raman amplification. The seed beam does not lengthen beyond the coherence time of the pump, even in the linear regime of amplification, but its final intensity and growth in the nonlinear regime are similar to those for a fully coherent pump. The plasma has density $N = 0.02$ and an electron temperature of 100 eV, with a central pump wavelength of 1 μm . The incoherent pump is constructed from the sum of one thousand components with a random phase and a Gaussian distribution of wavelength, the bandwidth of which corresponds to the pump coherence time.

different speeds in the medium, are no longer in phase on average and the seed does not grow. However, in the nonlinear regime, the pump is depleted on this scale anyway, so the overall effect on the seed dynamics is small.

In the linear regime, rather than growing substantially in length, the seed pulse will only lengthen to a scale comparable to the coherence time of the pump. The apparent growth rate will also be lower, as the peak of the pulse ordinarily drifts backwards as the pulse lengths. The modified dynamics for an incoherent pump are similar to those described by the quasitransient backward Raman amplification regime^{124,125} where the interaction is heavily damped within the time-scale of the seed pulse.

The resilience of plasma amplification to incoherence of the pump has a number of important implications for building plasma amplifiers. First, since spontaneous scattering grows in the linear regime and is relatively suppressed, an incoherent pump beam may reduce parasitic instabilities in a plasma amplifier. Second, since the plasma wave locally self-organizes to the phase of the seed, the seed remains coherent and the pump incoherence is deposited solely in the plasma wave; plasma amplification is, therefore, a method for cleaning the coherence of the pump beam, producing a high-quality output from a lower quality source. Finally, robustness to incoherence means that the quasi-coherent output of free electron lasers could, in principle, be suitable for pumping a plasma amplifier.

2. X-ray amplification

Equations (6)–(13) are normalized by the pump frequency, and in this form, the dominant terms are independent of wavelength. One of the advantages of plasma as an optical medium is that the light interacts with continuum electron energy levels, so responses are not strongly frequency-dependent and plasma amplifiers should be applicable to broad spectrum ranges. In particular, the difficulty in building traditional lasers at soft x-ray wavelengths has motivated consideration of plasmas as a potential amplification medium.^{117,126–129}

At shorter wavelengths, the primary change in dynamics is driven by damping; the window between strong Landau and collisional damping of the plasma wave that was open at visible

wavelengths begins to close for x-rays. This is a particular problem for Raman amplification, whose effective growth rate drops well below the effective growth rate of Brillouin amplification for soft x-rays. Figure 15 shows the effective growth rate of a seed pulse in a uniform plasma $T_e = 200$ eV at varied pump wavelengths and plasma densities. For Raman amplification [Fig. 15(a)], the growth rate rapidly drops off at lower densities due to Landau damping and goes to zero above $N = 0.25$. At shorter wavelengths, higher N becomes impractical due to collisional damping, resulting in the diagonal cutoff in the growth rate plot. Note that at fixed N and decreasing λ , the density in non-normalized units increases, resulting in the lower N at which collisional damping appears. Below $\lambda = 5$ nm, the gap between Landau and collisional damping closes and the growth rate at all densities drops to zero. In contrast, Brillouin amplification is somewhat more resilient to damping, and between $\lambda = 1 - 10$ nm, the growth rate remains reasonable, suggesting that the amplification of soft x-rays by SBS is possible.

3. Strongly magnetized plasma

The addition of a magnetic field to a plasma dramatically increases the number of waves and instabilities that may appear, and a number of recent works explore how external magnetic fields applied to a plasma change the laser-plasma interaction physics.^{119,129–131} As illustrated in Fig. 16, in addition to the Raman and Brillouin backscattering mechanisms, additional modes appear for coupling between counterpropagating light waves in a magnetized plasma, including Alfvén, lower hybrid, and upper hybrid waves, each distinguishable by different contributions from electrons, ions, and electric and magnetic field components.

Of interest for laser amplification is the presence of regions of strong coupling for specific plasma and magnetic field parameters. As a plot of backscattered spectra for different magnetic field strengths [Fig. 17(a)] shows, increasing the magnetic field dramatically changes the backscattered spectrum. In this plot, a pump beam ($\lambda = 1 \mu\text{m}$) enters a uniform underdense plasma, and the spectrum of light directly backscattered is recorded. At 100 T, with the magnetic field at $\theta_B = 85^\circ$ with respect to the incident pump propagation vector, the

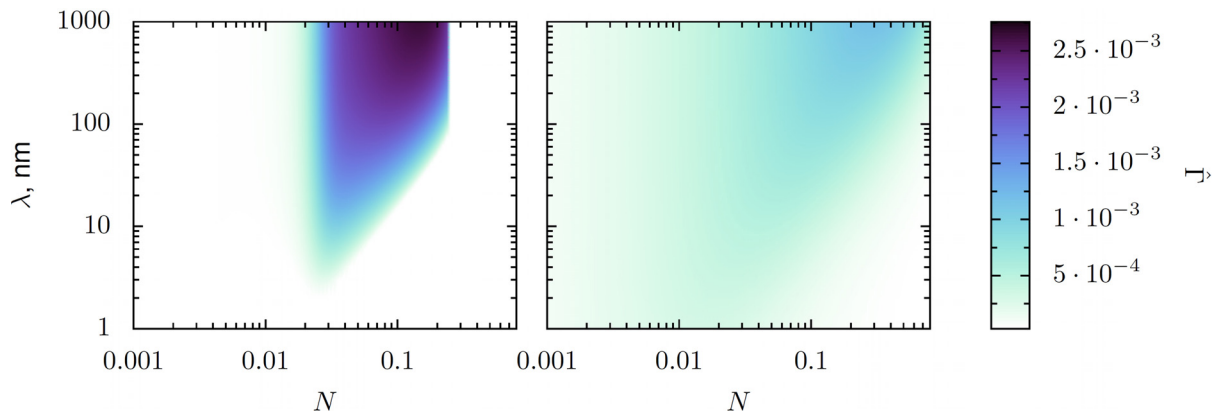


FIG. 15. Growth rate of a seed pulse amplified by stimulated Raman scattering (a) and stimulated Brillouin scattering (b) as a function of pump wavelength (λ) and normalized plasma density (N) at $T_e = 200$ eV. The growth rate is corrected for both Landau and collisional damping. The pump has $a_0 = 0.01$.

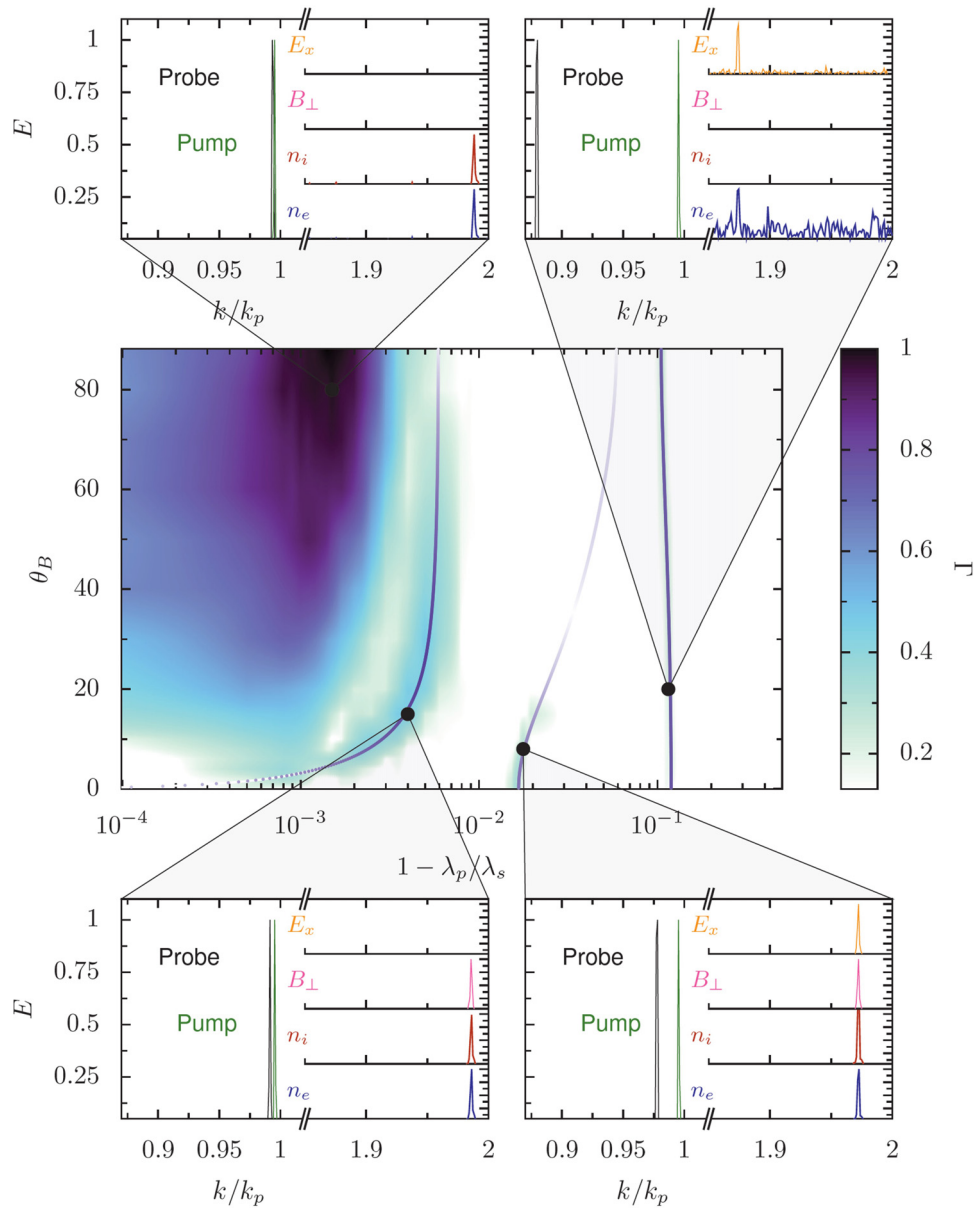


FIG. 16. Stimulated scattering modes in a magnetized plasma with low ion to electron mass. A pump beam and seed beam downshifted by $(\lambda_s - \lambda_p)$ counterpropagate in an underdense plasma, and the logarithmic gain of energy in the seed is plotted as a function of the seed wavelength and magnetic field angle with respect to the pump propagation direction. $B = 600$ T, $N = 0.01$, $T_e = T_i = 1$ eV, and $m_i/m_e = 10$. The low ion mass allows four modes to be distinguished: from left to right, the sound wave, the Alfvén wave, the lower hybrid, and the upper hybrid waves, with the solid lines showing analytic predictions.¹³⁰

main scattered light components are still Raman ($\omega/\omega_0 \approx 0.9$) and Brillouin ($\omega/\omega_0 \approx 1$). As the magnetic field increases and the cyclotron frequency becomes non-negligible, the source of Raman-type scattering changes from a Langmuir wave to an upper hybrid wave. Laser amplification is possible, showing some possibility for improvements in performance over unmagnetized plasma.¹²⁰

For magnetic field strengths where the cyclotron frequency is comparable to the pump laser frequency (here near 10 kT), extremely

strong scattering occurs from kinetic Alfvén waves. The magnetized low frequency (MLF) mechanism¹¹⁹ is characterized by a relatively small frequency downshift from the pump wave but a large growth rate. In comparison to a Raman amplified pulse, one growing by the MLF mechanism will much more quickly deplete its pump beam [Fig. 17(b)]. Although the magnetic fields required to see this mechanism are extremely large (>1 kT for $\lambda = 1 \mu\text{m}$), it has the characteristics of an ideal plasma mechanism for amplification: large growth rate

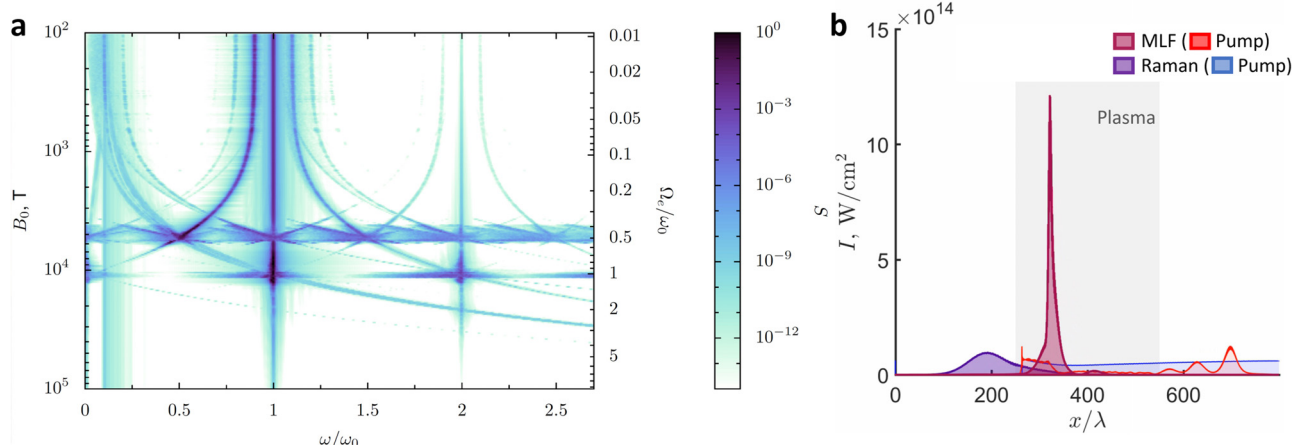


FIG. 17. (a) Spectral energy distribution of light backscattered from magnetized plasma ($\lambda = 1 \mu\text{m}$, $N = 0.01$, $T_e = T_i = 1 \text{ eV}$, and $m_i/m_e = 1836$) in PIC simulations. The magnetic field B_0 is varied between 100 T and 10 kT at $\theta_B = 85^\circ$. (b) Comparison of an amplified seed after propagation through a uniform plasma with (MLF) and without (Raman) a uniform magnetic field. The higher coupling in the magnetic field case leads to a more rapidly depleted pump.

and small frequency downshift, as well as support for broad bandwidth, extremely short amplified seed pulses.

IV. CONCLUSION

Plasmas allow control of light at extraordinary intensity. We can draw on their intrinsically high damage thresholds, fast response times, and a wealth of nonlinear responses to build optical components capable of supporting far higher fluxes than solid state devices. The two broad approaches discussed here—parametric plasma amplification and relativistic high-order harmonic generation—amplify high power pulses of light and efficiently convert light to new frequencies at high power, both of which are key capabilities for future plasma-based optical systems.

The primary application of parametric plasma amplification is the generation of laser-like pulses of light at intensities that would not be supported by solid gratings or in a solid amplifier. The process scales well with the wavelength and, if suitable pump beams are available, can be extended well into the infrared or toward x-ray wavelengths. Parametric amplification is resilient to incoherence in the driving beam and can also be used to produce a coherent pulse from an incoherent driving beam. The process is modified in the presence of a magnetic field: when the cyclotron frequency approaches the pump frequency, magnetized low frequency scattering from kinetic Alfvén waves offers exceptional amplification properties.

Relativistic high-order harmonic generation is particularly promising for producing light from extreme ultraviolet to soft x-ray wavelengths. With intrinsically coherent and supporting attosecond durations, RHHG is an ideal source for high peak power ultrashort pulses. The efficiency of RHHG, which can theoretically reach a $p = -4/3$ power law of frequency, can be improved by changing laser intensity, target density, or laser frequency. Effective changes in laser frequency can also be realized by a configuration of multiple sequential plasma mirrors, where each subsequent mirror adds to the frequency content of the beam.

The development of plasma sources of high intensity coherent light is necessary to advance beyond the limits of non-ionized media. Although there are many unsolved problems, particularly in translating theory to experiment, plasma sources remain a promising and necessary avenue for creating the next generation of bright light sources.

ACKNOWLEDGMENTS

This work was partially supported by the National Science Foundation under Grant No. PHY 1806911, the Department of Energy under Grant No. DE-SC0017907, the Department of Energy National Nuclear Security Administration under Grant No. DE-NA0003871, and the Lawrence Livermore National Laboratory LDRD Program (Grant No. 20-ERD-057). Lawrence Livermore National Laboratory is operated by Lawrence Livermore National Security, LLC, for the U.S. Department of Energy, National Nuclear Security Administration, under Contract No. DE-AC52-07NA27344.

APPENDIX: NOTES ON SIMULATIONS

The results presented in this paper are based heavily on one-dimensional particle-in-cell (PIC) simulations using the codes BOPS¹³² and EPOCH.¹³³ Both codes are relativistic and capture all three components of velocity; EPOCH additionally can be run in both two and three spatial dimensions. We used a relativistically boosted reference frame¹³⁴ to simulate HHG at oblique angles in 1D. BOPS has a built-in implementation of the relativistic boosting. In EPOCH, it is achieved via transforms of the input variables within the input file and appropriate transforms of the simulation output. For relativistic HHG simulations, the ions are usually assumed to be infinitely massive (unless otherwise noted), and the initial plasma is cold ($T_e = 0 \text{ eV}$). Table I shows the key computational parameters for PIC simulations presented throughout this paper.

TABLE I. Physical and computational parameters.

Figures	Code	Num. Sims. ^a	Cells/ λ^b	Part./Cell ^c
3	EPOCH	1	50 000	12
4	EPOCH	961	3000	15
5	EPOCH	10	1500	100
6	EPOCH	65	800	50
8	EPOCH	20	1200	5000
9	EPOCH	2	600	80
10(b)	BOPS	2	834	150
10(c)	BOPS	3	834	150
14	EPOCH	1	60	80
16	EPOCH	840	60	30
17(a)	EPOCH	300	50	40
17(b)	EPOCH	2	60	40

^aNumber of distinct simulations presented in the figure.

^bAll dimensional values are calculated using either $\lambda = 800$ nm or $\lambda = 1$ μ m, but with the neglect of atomic physics and appropriate non-dimensionalization simulation results are not λ -dependent. BOPS explicitly uses a wavelength-independent normalization for the calculations.

^cNumber of particles in a cell in regions where the plasma density is non-zero at the beginning of the simulation.

DATA AVAILABILITY

The data that support the findings of this study are available from the corresponding author upon reasonable request.

REFERENCES

- C. Geddes, C. Toth, J. Van Tilborg, E. Esarey, C. Schroeder, D. Bruhwiler, C. Nieter, J. Cary, and W. Leemans, "High-quality electron beams from a laser wakefield accelerator using plasma-channel guiding," *Nature* **431**, 538 (2004).
- W. P. Leemans, B. Nagler, A. J. Gonsalves, C. Toth, K. Nakamura, C. G. Geddes, E. Esarey, C. Schroeder, and S. Hooker, "GeV electron beams from a centimeter-scale accelerator," *Nat. Phys.* **2**, 696 (2006).
- E. Esarey, C. Schroeder, and W. Leemans, "Physics of laser-driven plasma-based electron accelerators," *Rev. Mod. Phys.* **81**, 1229 (2009).
- K. Schmid, A. Buck, C. M. Sears, J. M. Mikhailova, R. Tautz, D. Herrmann, M. Geissler, F. Krausz, and L. Veisz, "Density-transition based electron injector for laser driven wakefield accelerators," *Phys. Rev. Spec. Top.—Accel. Beams* **13**, 091301 (2010).
- A. Buck, M. Nicolai, K. Schmid, C. M. Sears, A. Sävert, J. M. Mikhailova, F. Krausz, M. C. Kaluza, and L. Veisz, "Real-time observation of laser-driven electron acceleration," *Nat. Phys.* **7**, 543 (2011).
- P. Gibbon, "Harmonic generation by femtosecond laser-solid interaction: A coherent 'water-window' light source?," *Phys. Rev. Lett.* **76**, 50 (1996).
- B. Dromey, S. Cousens, S. Rykovanov, M. Yeung, D. Jung, D. Gautier, T. Dzelzainis, D. Kiefer, S. Palaniyppan, R. Shah *et al.*, "Coherent synchrotron emission in transmission from ultrathin relativistic laser plasmas," *New J. Phys.* **15**, 015025 (2013).
- B. A. Remington, R. P. Drake, and D. D. Ryutov, "Experimental astrophysics with high power lasers and Z pinches," *Rev. Mod. Phys.* **78**, 755 (2006).
- F. Fiuza, R. Fonseca, J. Tonge, W. Mori, and L. Silva, "Weibel-instability-mediated collisionless shocks in the laboratory with ultraintense lasers," *Phys. Rev. Lett.* **108**, 235004 (2012).
- D. Strickland and G. Mourou, "Compression of amplified chirped optical pulses," *Opt. Commun.* **55**, 447–449 (1985).
- V. Malkin, Z. Toroker, and N. Fisch, "Saturation of the leading spike growth in backward Raman amplifiers," *Phys. Plasmas* **21**, 093112 (2014).
- M. Murnane, H. Kapteyn, and R. Falcone, "High-density plasmas produced by ultrafast laser pulses," *Phys. Rev. Lett.* **62**, 155 (1989).
- H. C. Kapteyn, M. M. Murnane, A. Szoke, and R. W. Falcone, "Prepulse energy suppression for high-energy ultrashort pulses using self-induced plasma shuttering," *Opt. Lett.* **16**, 490–492 (1991).
- S. Backus, H. C. Kapteyn, M. M. Murnane, D. M. Gold, H. Nathel, and W. White, "Prepulse suppression for high-energy ultrashort pulses using self-induced plasma shuttering from a fluid target," *Opt. Lett.* **18**, 134–136 (1993).
- C. Thauray, F. Quéré, J.-P. Geindre, A. Levy, T. Ceccotti, P. Monot, M. Bougeard, F. Réau, P. d'Oliveira, P. Audebert, R. Marjoribanks, and P. Martin, "Plasma mirrors for ultrahigh-intensity optics," *Nat. Phys.* **3**, 424–429 (2007).
- R. Lichters, J. Meyer-ter Vehn, and A. Pukhov, "Short-pulse laser harmonics from oscillating plasma surfaces driven at relativistic intensity," *Phys. Plasmas* **3**, 3425–3437 (1996).
- U. Teubner, G. Pretzler, T. Schlegel, K. Eidmann, E. Förster, and K. Witte, "Anomalies in high-order harmonic generation at relativistic intensities," *Phys. Rev. A* **67**, 013816 (2003).
- N. M. Naumova, J. A. Nees, I. V. Sokolov, B. Hou, and G. A. Mourou, "Relativistic generation of isolated attosecond pulses in a λ^3 focal volume," *Phys. Rev. Lett.* **92**, 063902 (2004).
- B. Dromey, M. Zepf, A. Gopal, K. Lancaster, M. Wei, K. Krushelnick, M. Tatarakis, N. Vakakis, S. Moustazis, R. Kodama, M. Tampo, C. Stoeckl, R. Clarke, H. Habara, D. Neely, S. Karsch, and P. Norreys, "High harmonic generation in the relativistic limit," *Nat. Phys.* **2**, 456–459 (2006).
- F. Quéré, C. Thauray, P. Monot, S. Dobos, P. Martin, J.-P. Geindre, and P. Audebert, "Coherent wake emission of high-order harmonics from overdense plasmas," *Phys. Rev. Lett.* **96**, 125004 (2006).
- C. Thauray and F. Quéré, "High-order harmonic and attosecond pulse generation on plasma mirrors: Basic mechanisms," *J. Phys. B: At., Mol. Opt. Phys.* **43**, 213001 (2010).
- J. M. Mikhailova, M. V. Fedorov, N. Karpowicz, P. Gibbon, V. T. Platonenko, A. M. Zheltikov, and F. Krausz, "Isolated attosecond pulses from laser-driven synchrotron radiation," *Phys. Rev. Lett.* **109**, 245005 (2012).
- P. Heissler, R. Hörlein, J. M. Mikhailova, L. Waldecker, P. Tzallas, A. Buck, K. Schmid, C. M. S. Sears, F. Krausz, L. Veisz, M. Zepf, and G. D. Tsakiris, "Few-cycle driven relativistically oscillating plasma mirrors: A source of intense isolated attosecond pulses," *Phys. Rev. Lett.* **108**, 235003 (2012).
- C. Rödel, D. an der Brügge, J. Bierbach, M. Yeung, T. Hahn, B. Dromey, S. Herzer, S. Fuchs, A. G. Pour, E. Eckner *et al.*, "Harmonic generation from relativistic plasma surfaces in ultrasteep plasma density gradients," *Phys. Rev. Lett.* **109**, 125002 (2012).
- V. M. Malkin, G. Shvets, and N. J. Fisch, "Fast compression of laser beams to highly overcritical powers," *Phys. Rev. Lett.* **82**, 4448–4451 (1999).
- A. Andreev, C. Riconda, V. Tikhonchuk, and S. Weber, "Short light pulse amplification and compression by stimulated Brillouin scattering in plasmas in the strong coupling regime," *Phys. Plasmas* **13**, 053110 (2006).
- W. Cheng, Y. Avitzour, Y. Ping, S. Suckewer, N. J. Fisch, M. S. Hur, and J. S. Wurtele, "Reaching the nonlinear regime of Raman amplification of ultrashort laser pulses," *Phys. Rev. Lett.* **94**, 045003 (2005).
- M. R. Edwards, Q. Jia, J. M. Mikhailova, and N. J. Fisch, "Short-pulse amplification by strongly-coupled stimulated Brillouin scattering," *Phys. Plasmas* **23**, 083122 (2016).
- R. Kirkwood, D. Turnbull, T. Chapman, S. Wilks, M. Rosen, R. London, L. Pickworth, W. Dunlop, J. Moody, D. Strozzi *et al.*, "Plasma-based beam combiner for very high fluence and energy," *Nat. Phys.* **14**, 80 (2018).
- P. Michel, L. Divol, D. Turnbull, and J. Moody, "Dynamic control of the polarization of intense laser beams via optical wave mixing in plasmas," *Phys. Rev. Lett.* **113**, 205001 (2014).
- K. Qu, Q. Jia, and N. J. Fisch, "Plasma q-plate for generation and manipulation of intense optical vortices," *Phys. Rev. E* **96**, 053207 (2017).
- D. Turnbull, P. Michel, T. Chapman, E. Tubman, B. Pollock, C. Chen, C. Goyon, J. Ross, L. Divol, N. Woolsey *et al.*, "High power dynamic polarization control using plasma photonics," *Phys. Rev. Lett.* **116**, 205001 (2016).
- D. Turnbull, C. Goyon, G. Kemp, B. Pollock, D. Mariscal, L. Divol, J. Ross, S. Patankar, J. Moody, and P. Michel, "Refractive index seen by a probe beam interacting with a laser-plasma system," *Phys. Rev. Lett.* **118**, 015001 (2017).

- ³⁴M. Kando, A. Pirozhkov, K. Kawase, T. Z. Esirkepov, Y. Fukuda, H. Kiriya, H. Okada, I. Daito, T. Kameshima, Y. Hayashi *et al.*, "Enhancement of photon number reflected by the relativistic flying mirror," *Phys. Rev. Lett.* **103**, 235003 (2009).
- ³⁵J. Dias, C. Stenz, N. Lopes, X. Badiche, F. Blasco, A. Dos Santos, L. O. e Silva, A. Mysyrowicz, A. Antonetti, and J. Mendonça, "Experimental evidence of photon acceleration of ultrashort laser pulses in relativistic ionization fronts," *Phys. Rev. Lett.* **78**, 4773 (1997).
- ³⁶C. D. Murphy, R. M. G. M. Trines, J. Vieira, A. J. W. Reitsma, R. Bingham, J. L. Collier, E. J. Divall, P. S. Foster, C. J. Hooker, A. J. Langley *et al.*, "Evidence of photon acceleration by laser wake fields," *Phys. Plasmas* **13**, 033108 (2006).
- ³⁷M. Edwards, K. Qu, Q. Jia, J. M. Mikhailova, and N. J. Fisch, "Cascaded chirped photon acceleration for efficient frequency conversion," *Phys. Plasmas* **25**, 053102 (2018).
- ³⁸K. Qu, Q. Jia, M. R. Edwards, and N. J. Fisch, "Theory of electromagnetic wave frequency upconversion in dynamic media," *Phys. Rev. E* **98**, 023202 (2018).
- ³⁹A. Howard, D. Turnbull, A. Davies, P. Franke, D. Froula, and J. Palastro, "Photon acceleration in a flying focus," *Phys. Rev. Lett.* **123**, 124801 (2019).
- ⁴⁰F. Albert, A. Thomas, S. Mangles, S. Banerjee, S. Corde, A. Flacco, M. Litos, D. Neely, J. Vieira, Z. Najmudin *et al.*, "Laser wakefield accelerator based light sources: Potential applications and requirements," *Plasma Phys. Controlled Fusion* **56**, 084015 (2014).
- ⁴¹F. Albert and A. G. Thomas, "Applications of laser wakefield accelerator-based light sources," *Plasma Phys. Controlled Fusion* **58**, 103001 (2016).
- ⁴²M. Hentschel, R. Kienberger, C. Spielmann, G. A. Reider, N. Milosevic, T. Brabec, P. Corkum, U. Heinzmann, M. Drescher, and F. Krausz, "Attosecond metrology," *Nature* **414**, 509 (2001).
- ⁴³J. L. Krause, K. J. Schafer, and K. C. Kulander, "High-order harmonic generation from atoms and ions in the high intensity regime," *Phys. Rev. Lett.* **68**, 3535 (1992).
- ⁴⁴P. B. Corkum, "Plasma perspective on strong field multiphoton ionization," *Phys. Rev. Lett.* **71**, 1994 (1993).
- ⁴⁵G. Sansone, E. Benedetti, F. Calegari, C. Vozzi, L. Avaldi, R. Flammini, L. Poletto, P. Villorosi, C. Altucci, R. Velotta *et al.*, "Isolated single-cycle attosecond pulses," *Science* **314**, 443–446 (2006).
- ⁴⁶P. M. Paul, E. Toma, P. Breger, G. Mullot, F. Augé, P. Balcou, H. Muller, and P. Agostini, "Observation of a train of attosecond pulses from high harmonic generation," *Science* **292**, 1689–1692 (2001).
- ⁴⁷M. Drescher, M. Hentschel, R. Kienberger, G. Tempea, C. Spielmann, G. A. Reider, P. B. Corkum, and F. Krausz, "X-ray pulses approaching the attosecond frontier," *Science* **291**, 1923–1927 (2001).
- ⁴⁸R. Ganeev, L. E. Bom, J. Abdul-Hadi, M. Wong, J. Brichta, V. Bhardwaj, and T. Ozaki, "Higher-order harmonic generation from fullerene by means of the plasma harmonic method," *Phys. Rev. Lett.* **102**, 013903 (2009).
- ⁴⁹S. Ghimire, A. D. DiChiara, E. Sistrunk, P. Agostini, L. F. DiMauro, and D. A. Reis, "Observation of high-order harmonic generation in a bulk crystal," *Nat. Phys.* **7**, 138 (2011).
- ⁵⁰G. Vampa, C. McDonald, G. Orlando, D. Klug, P. Corkum, and T. Brabec, "Theoretical analysis of high-harmonic generation in solids," *Phys. Rev. Lett.* **113**, 073901 (2014).
- ⁵¹T. Higuchi, M. I. Stockman, and P. Hommelhoff, "Strong-field perspective on high-harmonic radiation from bulk solids," *Phys. Rev. Lett.* **113**, 213901 (2014).
- ⁵²P. Norreys, M. Zepf, S. Moustazis, A. Fewes, J. Zhang, P. Lee, M. Bakarezos, C. Danson, A. Dyson, P. Gibbon *et al.*, "Efficient extreme UV harmonics generated from picosecond laser pulse interactions with solid targets," *Phys. Rev. Lett.* **76**, 1832 (1996).
- ⁵³I. Watts, M. Zepf, E. Clark, M. Tatarakis, K. Krushelnick, A. Dangor, R. Allott, R. Clarke, D. Neely, and P. Norreys, "Dynamics of the critical surface in high-intensity laser-solid interactions: Modulation of the XUV harmonic spectra," *Phys. Rev. Lett.* **88**, 155001 (2002).
- ⁵⁴F. Dollar, P. Cummings, V. Chvykov, L. Willingale, M. Vargas, V. Yanovsky, C. Zulfick, A. Maksimchuk, A. Thomas, and K. Krushelnick, "Scaling high-order harmonic generation from laser-solid interactions to ultrahigh intensity," *Phys. Rev. Lett.* **110**, 175002 (2013).
- ⁵⁵S. Kahaly, S. Monchocé, H. Vincenti, T. Dzelzainis, B. Dromey, M. Zepf, P. Martin, and F. Quéré, "Direct observation of density-gradient effects in harmonic generation from plasma mirrors," *Phys. Rev. Lett.* **110**, 175001 (2013).
- ⁵⁶P. Heissler, A. Barna, J. M. Mikhailova, G. Ma, K. Khrennikov, S. Karsch, L. Veisz, I. Földes, and G. D. Tsakiris, "Multi- μ J harmonic emission energy from laser-driven plasma," *Appl. Phys. B* **118**, 195–201 (2015).
- ⁵⁷M. Yeung, S. Rykovanov, J. Bierbach, L. Li, E. Eckner, S. Kuschel, A. Woldegeorgis, C. Rödel, A. Sävert, G. Paulus *et al.*, "Experimental observation of attosecond control over relativistic electron bunches with two-colour fields," *Nat. Photonics* **11**, 32–35 (2017).
- ⁵⁸T. Baeva, S. Gordienko, and A. Pukhov, "Theory of high-order harmonic generation in relativistic laser interaction with overdense plasma," *Phys. Rev. E* **74**, 046404 (2006).
- ⁵⁹A. A. Gonoskov, A. V. Korzhimanov, A. V. Kim, M. Marklund, and A. M. Sergeev, "Ultrarelativistic nanoplasmons as a route towards extreme-intensity attosecond pulses," *Phys. Rev. E* **84**, 046403 (2011).
- ⁶⁰T. Blackburn, A. Gonoskov, and M. Marklund, "Relativistically intense XUV radiation from laser-illuminated near-critical plasmas," *Phys. Rev. A* **98**, 023421 (2018).
- ⁶¹A. Gonoskov, "Theory of relativistic radiation reflection from plasmas," *Phys. Plasmas* **25**, 013108 (2018).
- ⁶²D. an der Brügge and A. Pukhov, "Enhanced relativistic harmonics by electron nanobunching," *Phys. Plasmas* **17**, 033110 (2010).
- ⁶³B. Dromey, S. Rykovanov, M. Yeung, R. Hörlein, D. Jung, D. Gautier, T. Dzelzainis, D. Kiefer, S. Palaniyppan, R. Shah *et al.*, "Coherent synchrotron emission from electron nanobunches formed in relativistic laser-plasma interactions," *Nat. Phys.* **8**, 804–808 (2012).
- ⁶⁴M. R. Edwards and J. M. Mikhailova, "The x-ray emission effectiveness of plasma mirrors: Reexamining power-law scaling for relativistic high-order harmonic generation," *Sci. Rep.* **10**, 5154 (2020).
- ⁶⁵M. R. Edwards, "Ultrafast sources of intense radiation," Ph.D. thesis (Princeton University, 2019).
- ⁶⁶ $\int_1^\infty \omega^{-4/3} d\omega = 3$.
- ⁶⁷S. Gordienko and A. Pukhov, "Scalings for ultrarelativistic laser plasma and quasimonochromatic electrons," *Phys. Plasmas* **12**, 043109 (2005).
- ⁶⁸A. Pukhov and S. Gordienko, "Bubble regime of wake field acceleration: Similarity theory and optimal scalings," *Philos. Trans. R. Soc., A* **364**, 623–633 (2006).
- ⁶⁹D. D. Ryutov and B. A. Remington, "Similarity laws for collisionless interaction of superstrong electromagnetic fields with a plasma," *Plasma Phys. Controlled Fusion* **48**, L23–L31 (2006).
- ⁷⁰A. Tarasevitch, K. Lobov, C. Wünsche, and D. von der Linde, "Transition to the relativistic regime in high order harmonic generation," *Phys. Rev. Lett.* **98**, 103902 (2007).
- ⁷¹S. Bhandarkar, T. Baumann, N. Alfonso, C. Thomas, K. Baker, A. Moore, C. Larson, D. Bennett, J. Sain, and A. Nikroo, "Fabrication of low-density foam liners in Hohlraums for NIF targets," *Fusion Sci. Technol.* **73**, 194–209 (2018).
- ⁷²Y. M. Mikhailova, V. T. Platonenko, and S. Rykovanov, "Generation of an attosecond x-ray pulse in a thin film irradiated by an ultrashort ultrarelativistic laser pulse," *JETP Lett.* **81**, 571–574 (2005).
- ⁷³J. M. Mikhailova and V. T. Platonenko, "Efficient generation of attosecond x-ray radiation under interaction of ultrarelativistic few-cycle laser pulse with a thin foil," *AIP Conf. Proc.* **827**, 429–435 (2006).
- ⁷⁴M. R. Edwards, N. M. Fasano, and J. M. Mikhailova, "Electron-nanobunch-width-dominated spectral power law for relativistic harmonic generation from ultrathin foils," *Phys. Rev. Lett.* **124**, 185004 (2020).
- ⁷⁵M. R. Edwards, V. T. Platonenko, and J. M. Mikhailova, "Enhanced attosecond bursts of relativistic high-order harmonics driven by two-color fields," *Opt. Lett.* **39**, 6823–6826 (2014).
- ⁷⁶Although polarization for each beam is in principle also a free parameter, efficiency is highest when all component colors are p polarized, just as in the single-frequency case.
- ⁷⁷M. R. Edwards and J. M. Mikhailova, "Waveform-controlled relativistic high-order-harmonic generation," *Phys. Rev. Lett.* **117**, 125001 (2016).

- ⁷⁸P. Zhang and A. Thomas, "Enhancement of high-order harmonic generation in intense laser interactions with solid density plasma by multiple reflections and harmonic amplification," *Appl. Phys. Lett.* **106**, 131102 (2015).
- ⁷⁹M. R. Edwards and J. M. Mikhailova, "Multipass relativistic high-order harmonic generation for intense attosecond pulses," *Phys. Rev. A* **93**, 023836 (2016).
- ⁸⁰Z. Léczy and A. Andreev, "Enhancement of high harmonic generation by multiple reflection of ultrashort pulses," *J. Opt. Soc. Am. B* **35**, A49–A55 (2018).
- ⁸¹M. R. Edwards, N. M. Fasano, T. Bennett, A. Griffith, N. Turley, B. M. O'Brien, and J. M. Mikhailova, "Cascaded plasma mirrors for enhanced relativistic harmonic generation," in *CLEO: Fundamental Science*, San Jose, CA, 11–15 May 2020.
- ⁸²S. Tietze, M. Zepf, S. G. Rykovanov, and M. Yeung, "Propagation effects in multipass high harmonic generation from plasma surfaces," *New J. Phys.* **22**, 093048 (2020).
- ⁸³M. R. Edwards, N. M. Fasano, T. Bennett, A. Griffith, N. Turley, B. M. O'Brien, and J. M. Mikhailova, "A multi-terawatt two-color beam for high-power field-controlled nonlinear optics," *Opt. Lett.* **45**, 6542–6545 (2020).
- ⁸⁴J.-R. Marquès, L. Lancia, T. Gangolf, M. Blecher, S. Bolaños, J. Fuchs, O. Willi, F. Amiranoff, R. Berger, M. Chieramello *et al.*, "Joule-level high-efficiency energy transfer to subpicosecond laser pulses by a plasma-based amplifier," *Phys. Rev. X* **9**, 021008 (2019).
- ⁸⁵Y. Ping, I. Geltner, A. Morozov, N. Fisch, and S. Suckewer, "Raman amplification of ultrashort laser pulses in microcapillary plasmas," *Phys. Rev. E* **66**, 046401 (2002).
- ⁸⁶Y. Ping, W. Cheng, S. Suckewer, D. S. Clark, and N. J. Fisch, "Amplification of ultrashort laser pulses by a resonant Raman scheme in a gas-jet plasma," *Phys. Rev. Lett.* **92**, 175007 (2004).
- ⁸⁷R. Kirkwood, E. Dewald, C. Niemann, N. Meezan, S. Wilks, D. Price, O. Landen, J. Wurtele, A. Charman, R. Lindberg, N. Fisch, V. Malkin, and E. Valeo, "Amplification of an ultrashort pulse laser by stimulated Raman scattering of a 1 ns pulse in a low density plasma," *Phys. Plasmas* **14**, 113109 (2007).
- ⁸⁸J. Ren, S. Li, A. Morozov, S. Suckewer, N. Yampolsky, V. Malkin, and N. Fisch, "A compact double-pass Raman backscattering amplifier/compressor," *Phys. Plasmas* **15**, 056702 (2008).
- ⁸⁹Y. Ping, R. Kirkwood, T.-L. Wang, D. Clark, S. Wilks, N. Meezan, R. Berger, J. Wurtele, N. Fisch, V. Malkin *et al.*, "Development of a nanosecond-laser-pumped Raman amplifier for short laser pulses in plasma," *Phys. Plasmas* **16**, 123113 (2009).
- ⁹⁰D. Turnbull, S. Li, A. Morozov, and S. Suckewer, "Possible origins of a time-resolved frequency shift in Raman plasma amplifiers," *Phys. Plasmas* **19**, 073103 (2012).
- ⁹¹G. Vieux, A. Lyachev, X. Yang, B. Ersfeld, J. Farmer, E. Brunetti, R. Issac, G. Raj, G. Welsh, S. Wiggins *et al.*, "Chirped pulse Raman amplification in plasma," *New J. Phys.* **13**, 063042 (2011).
- ⁹²X. Yang, Z. Xu, Y. Leng, H. Lu, L. Lin, Z. Zhang, R. Li, W. Zhang, D. Yin, and B. Tang, "Multiterawatt laser system based on optical parametric chirped pulse amplification," *Opt. Lett.* **27**, 1135–1137 (2002).
- ⁹³L. Lancia, J.-R. Marquès, M. Nakatsutsumi, C. Riconda, S. Weber, S. Hüller, A. Mančić, P. Antici, V. Tikhonchuk, A. Héron *et al.*, "Experimental evidence of short light pulse amplification using strong-coupling stimulated Brillouin scattering in the pump depletion regime," *Phys. Rev. Lett.* **104**, 025001 (2010).
- ⁹⁴L. Lancia, A. Giribono, L. Vassura, M. Chieramello, C. Riconda, S. Weber, A. Castan, A. Chatelain, A. Frank, T. Gangolf, M. N. Quinn, J. Fuchs, and J.-R. Marquès, "Signatures of the self-similar regime of strongly coupled stimulated Brillouin scattering for efficient short laser pulse amplification," *Phys. Rev. Lett.* **116**, 075001 (2016).
- ⁹⁵E. Guillaume, K. Humphrey, H. Nakamura, R. Trines, R. Heathcote, M. Galimberti, Y. Amano, D. Doria, G. Hicks, E. Higson *et al.*, "Demonstration of laser pulse amplification by stimulated Brillouin scattering," *High Power Laser Sci. Eng.* **2**, e33 (2014).
- ⁹⁶M. Dreher, E. Takahashi, J. Meyer-ter Vehn, and K.-J. Witte, "Observation of superradiant amplification of ultrashort laser pulses in a plasma," *Phys. Rev. Lett.* **93**, 095001 (2004).
- ⁹⁷M. R. Edwards, N. J. Fisch, and J. M. Mikhailova, "Strongly enhanced stimulated Brillouin backscattering in an electron-positron plasma," *Phys. Rev. Lett.* **116**, 015004 (2016).
- ⁹⁸F. Schluck, G. Lehmann, and K. Spatschek, "Parametric pulse amplification by acoustic quasimodes in electron-positron plasma," *Phys. Rev. E* **96**, 053204 (2017).
- ⁹⁹V. Malkin, Y. A. Tsidulko, and N. Fisch, "Stimulated Raman scattering of rapidly amplified short laser pulses," *Phys. Rev. Lett.* **85**, 4068 (2000).
- ¹⁰⁰N. Yampolsky, N. Fisch, V. Malkin, E. Valeo, R. Lindberg, J. Wurtele, J. Ren, S. Li, A. Morozov, and S. Suckewer, "Demonstration of detuning and wave-breaking effects on Raman amplification efficiency in plasma," *Phys. Plasmas* **15**, 113104 (2008).
- ¹⁰¹N. A. Yampolsky and N. J. Fisch, "Limiting effects on laser compression by resonant backward Raman scattering in modern experiments," *Phys. Plasmas* **18**, 056711 (2011).
- ¹⁰²R. M. G. M. Trines, F. Fiúza, R. Bingham, R. A. Fonseca, L. O. Silva, R. A. Cairns, and P. A. Norreys, "Production of picosecond, kilojoule, and petawatt laser pulses via Raman amplification of nanosecond pulses," *Phys. Rev. Lett.* **107**, 105002 (2011).
- ¹⁰³R. Trines, F. Fiúza, R. Bingham, R. Fonseca, L. Silva, R. Cairns, and P. Norreys, "Simulations of efficient Raman amplification into the multipetawatt regime," *Nat. Phys.* **7**, 87 (2011).
- ¹⁰⁴S. Depierreux, V. Yahia, C. Goyon, G. Loisel, P.-E. Masson-Laborde, N. Borisenko, A. Orekhov, O. Rosmej, T. Rienecker, and C. Labaune, "Laser light triggers increased Raman amplification in the regime of nonlinear Landau damping," *Nat. Commun.* **5**, 4158 (2014).
- ¹⁰⁵Z. Toroker, V. Malkin, and N. Fisch, "Backward Raman amplification in the Langmuir wavebreaking regime," *Phys. Plasmas* **21**, 113110 (2014).
- ¹⁰⁶G. Lehmann and K. Spatschek, "Non-filamentated ultra-intense and ultrashort pulse fronts in three-dimensional Raman seed amplification," *Phys. Plasmas* **21**, 053101 (2014).
- ¹⁰⁷M. R. Edwards, Z. Toroker, J. M. Mikhailova, and N. J. Fisch, "The efficiency of Raman amplification in the wavebreaking regime," *Phys. Plasmas* **22**, 074501 (2015).
- ¹⁰⁸M. R. Edwards, K. Qu, J. M. Mikhailova, and N. J. Fisch, "Beam cleaning of an incoherent laser via plasma Raman amplification," *Phys. Plasmas* **24**, 103110 (2017).
- ¹⁰⁹R. M. G. M. Trines, E. P. Alves, E. Webb, J. Vieira, F. Fiúza, R. A. Fonseca, L. O. Silva, R. A. Cairns, and R. Bingham, "New criteria for efficient Raman and Brillouin amplification of laser beams in plasma," *Sci. Rep.* **10**, 19875 (2020).
- ¹¹⁰G. Lehmann, F. Schluck, and K. H. Spatschek, "Regions for Brillouin seed pulse growth in relativistic laser-plasma interaction," *Phys. Plasmas* **19**, 093120 (2012).
- ¹¹¹G. Lehmann and K. Spatschek, "Nonlinear Brillouin amplification of finite-duration seeds in the strong coupling regime," *Phys. Plasmas* **20**, 073112 (2013).
- ¹¹²S. Weber, C. Riconda, L. Lancia, J.-R. Marquès, G. A. Mourou, and J. Fuchs, "Amplification of ultrashort laser pulses by Brillouin backscattering in plasmas," *Phys. Rev. Lett.* **111**, 055004 (2013).
- ¹¹³C. Riconda, S. Weber, L. Lancia, J.-R. Marquès, G. A. Mourou, and J. Fuchs, "Spectral characteristics of ultra-short laser pulses in plasma amplifiers," *Phys. Plasmas* **20**, 083115 (2013).
- ¹¹⁴G. Lehmann and K. Spatschek, "Temperature dependence of seed pulse amplitude and density grating in Brillouin amplification," *Phys. Plasmas* **23**, 023107 (2016).
- ¹¹⁵M. Chieramello, F. Amiranoff, C. Riconda, and S. Weber, "Role of frequency chirp and energy flow directionality in the strong coupling regime of Brillouin-based plasma amplification," *Phys. Rev. Lett.* **117**, 235003 (2016).
- ¹¹⁶Q. Jia, I. Barth, M. R. Edwards, J. M. Mikhailova, and N. J. Fisch, "Distinguishing Raman from strongly coupled Brillouin amplification for short pulses," *Phys. Plasmas* **23**, 053118 (2016).
- ¹¹⁷M. R. Edwards, J. M. Mikhailova, and N. J. Fisch, "X-ray amplification by stimulated Brillouin scattering," *Phys. Rev. E* **96**, 023209 (2017).
- ¹¹⁸G. Shvets, N. Fisch, A. Pukhov, and J. Meyer-ter Vehn, "Superradiant amplification of an ultrashort laser pulse in a plasma by a counterpropagating pump," *Phys. Rev. Lett.* **81**, 4879–4882 (1998).

- ¹¹⁹M. R. Edwards, Y. Shi, J. M. Mikhailova, and N. J. Fisch, "Laser amplification in strongly magnetized plasma," *Phys. Rev. Lett.* **123**, 025001 (2019).
- ¹²⁰Q. Jia, Y. Shi, H. Qin, and N. J. Fisch, "Kinetic simulations of laser parametric amplification in magnetized plasmas," *Phys. Plasmas* **24**, 093103 (2017).
- ¹²¹H. Komine, W. H. Long, E. A. Stappaerts, and S. J. Brosnan, "Beam cleanup and low-distortion amplification in efficient high-gain hydrogen Raman amplifiers," *J. Opt. Soc. Am. B* **3**, 1428–1447 (1986).
- ¹²²R. Chang, R. Lehmborg, M. Duignan, and N. Djeu, "Raman beam cleanup of a severely aberrated pump laser," *IEEE J. Quantum Electron.* **21**, 477–487 (1985).
- ¹²³D. Borlaug, R. R. Rice, and B. Jalali, "Raman beam cleanup in silicon in the mid-infrared," *Opt. Express* **18**, 12411–12414 (2010).
- ¹²⁴V. M. Malkin and N. J. Fisch, "Quasitransient regimes of backward Raman amplification of intense x-ray pulses," *Phys. Rev. E* **80**, 046409 (2009).
- ¹²⁵V. Malkin and N. Fisch, "Quasitransient backward Raman amplification of powerful laser pulses in dense plasmas with multicharged ions," *Phys. Plasmas* **17**, 073109 (2010).
- ¹²⁶V. M. Malkin and N. J. Fisch, "Relic crystal-lattice effects on Raman compression of powerful x-ray pulses in plasmas," *Phys. Rev. Lett.* **99**, 205001 (2007).
- ¹²⁷V. M. Malkin, N. J. Fisch, and J. S. Wurtele, "Compression of powerful x-ray pulses to attosecond durations by stimulated Raman backscattering in plasmas," *Phys. Rev. E* **75**, 026404 (2007).
- ¹²⁸J. D. Sadler, R. Nathvani, P. Oleskiewicz, L. A. Ceurvorst, N. Ratan, M. F. Kasim, R. M. G. M. Trines, R. Bingham, and P. A. Norreys, "Compression of x-ray free electron laser pulses to attosecond duration," *Sci. Rep.* **5**, 16755 (2015).
- ¹²⁹Y. Shi, H. Qin, and N. J. Fisch, "Laser pulse compression using magnetized plasmas," *Phys. Rev. E* **95**, 023211 (2017).
- ¹³⁰Y. Shi, H. Qin, and N. J. Fisch, "Three-wave scattering in magnetized plasmas: From cold fluid to quantized Lagrangian," *Phys. Rev. E* **96**, 023204 (2017).
- ¹³¹Y. Shi, H. Qin, and N. J. Fisch, "Laser-plasma interactions in magnetized environment," *Phys. Plasmas* **25**, 055706 (2018).
- ¹³²P. Gibbon, A. Andreev, E. Lefebvre, G. Bonnaud, H. Ruhl, J. Delettrez, and A. Bell, "Calibration of one-dimensional boosted kinetic codes for modeling high-intensity laser-solid interactions," *Phys. Plasmas* **6**, 947–953 (1999).
- ¹³³T. D. Arber, K. Bennett, C. S. Brady, A. Lawrence-Douglas, M. G. Ramsay, N. J. Sircombe, P. Gillies, R. G. Evans, H. Schmitz, A. R. Bell, and C. P. Ridgers, "Contemporary particle-in-cell approach to laser-plasma modelling," *Plasma Phys. Controlled Fusion* **57**, 113001 (2015).
- ¹³⁴A. Bourdier, "Oblique incidence of a strong electromagnetic wave on a cold inhomogeneous electron plasma. Relativistic effects," *Phys. Fluids* **26**, 1804–1807 (1983).